Digest Journal of Nanomaterials and Biostructures Vol. 10, No. 1, January - March 2015, p. 59 - 87

Tuning the properties of Ge and Si nanocrystals based structures by tailoring the preparation conditions

Review

M. L. CIUREA, A.M. LEPADATU*
National Institute of Materials Physics, 105 bis Atomistilor Street, Magurele 077125, Romania

Ge and Si nanocrystals (NCs), quantum dots (QDs), and amorphous nanoparticles (NPs) have a significant role in the developement of micro- and nanoelectronic devices due to capability to tune their electrical and photoconductive properties by tailoring the morphology and structure parameters. Ge and Si NCs/QDs/NPs are zero-dimensional (0D) systems and the SiO_2 films containing them are percolative systems. In this review, the role of deposition and annealing conditions in the morphology and structure of Ge and Si NCs/QDs/NPs embedded in amorphous SiO_2 matrix is discussed for a wide variety of films and multilayered structures. The electrical and photoconductive properties of nanostructures deposited by different techniques as magnetron sputtering, ion implantation, chemical vapour deposition, sol-gel and molecular beam epitaxy, and subsequently annealed in conventional furnace or by rapid thermal annealing under different conditions are analised. We demonstrate how the electrical and photoconductive properties of nanostructures can be tuned by varying the deposition and annealing parameters. The role of Si-rich oxide and defects in the formation of Ge and Si NCs is shown and the role of defects in improving electrical properties and enhancing the photoconductivity of films and multilayered structures is highlighted. We evidence the contribution of quantum confinement effect and show that the most probable transport mechanisms in these percolative systems are tunnelling and hopping.

(Received November 3, 2014; Accepted December 18, 2014)

Keywords: Ge and Si nanocrystals; multilayers; deposition and annealing; electrical properties; photoconduction.

1. Introduction

It is well known that the nanostructures have different properties in respect of corresponding bulk materials due to the size effect [1−6]. In different nanostructures (nanocrystals, nanowires and quantum wells) the quantum confinement has two effects, namely the enlargement of the band gap of materials and the change of an indirect band gap toward a direct one. In the most of cases, these effects lead to superior properties of nanostructures, for example they enhance the photoluminescence and photocurrent with few orders of magnitude with respect to corresponding bulk materials.

The term of nanocrystal (NC) is used in the literature for crystalline nanoparticles (NPs) with sizes from nm to tens of nm or even higher. The NCs with size less than the exciton Bohr radius are usually called quantum dots (QDs) [5]. The QDs and small NCs present strong quantum confinement and therefore they have a great advantage as their size, density, shape and crystallinity can be tailored [4, 7−11] leading to different properties and consequently to a large variety of applications [12−18]. The potential applications of films containing Si and Ge NCs and QDs in nonvolatile memory devices [5, 19, 20], solar cells [1, 21−23], efficient light emitters [5,

* Corresponding author: lepadatu@infim.ro

22, 24, 25] and optical sensors [26−29] represent the driving force for improving the preparation conditions of these films and nanostructures and for studying their properties [30, 31]. For example, the electrical, photoconductive and optical properties of films containing Ge and Si NCs and QDs can be tuned by tailoring their size, density, shape, crystalline structure, surrounding dielectric matrix, and also by controlling the localized states formed at the interfaces between NCs/QDs and matrix [32−39]. These films contain internal strains (tensile or compressive) that can strongly influence the properties improving or hindering them [26, 40−42]. The key point in applications is to tailor the NCs size, to adjust their density and to grow NCs/QDs/NPs in predetermined fixed positions, in order to obtain the targeted properties. Thus, Ge NCs based photodetectors with high figures of merit (i.e. low dark current and high responsivity in the wavelength range of interest) were reported. The sizes of Ge NCs were tailored between 7 and 50 nm, and in this way the sensitivity was tuned from ultraviolet to near infrared [26]. Also, the photoluminescence emission in the films containing Ge and Si NCs depends on their size, being due to free exciton recombination within the Ge NCs [5, 33].

One route to obtain nanostructured films with adequate properties for targeted applications is to prepare Ge and Si NCs embedded in dielectrics [26, 43] by using the magnetron sputtering deposition method followed by annealing for films nanostructuring, i.e. for NCs formation. The films of Ge or Si NCs or amorphous NPs embedded in SiO_2 matrix are a particular case [44−50]. The films with targeted properties can be obtained by adjusting the size of NCs and choosing a suitable Ge concentration. In the case of very thin layers the NCs size is controlled by the film thickness (5 – 20 nm) [26].

Besides magnetron sputtering, which is the most used deposition method, other methods as ion implantation [51−55], plasma-enhanced chemical vapour deposition (CVD) [56−59], sol-gel [29, 45, 60−62], molecular beam epitaxy (MBE) [63, 64] etc., are used for the preparation of SiO_2 films with embedded NCs of Ge and Si.

In this paper we show how the electrical and photoconductive properties of films formed of Ge or Si NCs, QDs or NPs embedded in amorphous SiO_2 matrix can be tuned by modifying the preparation (deposition and annealing) conditions that determine the film structure and morphology. These films are percolative systems, and therefore, the electronic mechanisms which govern the electrical behaviour are essentially tunnelling or hopping. In the case of films with high photoconductive properties, the trapping centres play an important role in the transport mechanism. Here, we evidence the strong correlation between structure, electrical and photoconductive properties and we demonstrate the relevance of controlling the deposition and annealing parameters for obtaining films with desired structures and targeted electrical and photoconductive properties.

2. Influence of preparation conditions on structure and morphology of SiO_2 films with Ge or Si NCs or NPs

2.1. Influence of deposition conditions on film structure and morphology

In order to obtain films with Ge or Si NCs/QDs/NPs embedded in amorphous SiO_2 matrix, firstly Ge-SiO_2 and Si-SiO_2 films or multilayers are deposited. The deposition methods are magnetron sputtering [44, 46−50, 65−74], ion implantation [51−55, 75−80], plasma-enhanced CVD [30, 56−59, 81−84], sol-gel [29, 45, 60−62, 85−91] and MBE [63, 64, 92]. In the literature there are also reports on films and multilayers formed of Ge or Si NCs/NPs embedded in oxide, prepared by thermal evaporation, electron beam evaporation [93−96], and pulsed laser deposition [97].

2.1.1. Magnetron sputtering

This method is versatile and permits to vary different deposition parameters like substrate temperature during the process [46, 48, 65], Ge or Si concentration in respect to SiO_2 [45, 49, 68] and ambient gases (H_2 or O_2) concentration in the case of reactive sputtering [48, 65] etc. For example, films and multilayers of Ge-SiO_2 are deposited on substrates heated at temperatures between 250 and 400 ^oC [46, 65] and the as-deposited films contain Ge clusters and QDs. Usually,

if the substrate is maintained at room temperature (RT), the as-deposited films are amorphous. The deposition time determines the films thickness, and in the case of very thin films, i.e. two-dimensional (2D) systems also determines the size of NCs, as mentioned above [66, 98]. The oxygen partial pressure in the reactive sputtering process controls the stoichiometry and texture of SiO_2 films and the size and crystalline structure (cubic or tetragonal) of Ge NCs in SiO_2/Ge/SiO_2/Si multilayered structures [65]. In the case of non-reactive magnetron sputtering the size of Ge or Si NCs is influenced by Ge or Si concentrations in Ge-SiO_2 films or Si-SiO_2 films, respectively [49, 67, 68, 71]. For example, in SiO_x/SiO_2 multilayers (with $x < 2$) deposited on Si or quartz substrates, the size and density of Si QDs are controlled by the composition x of Si-rich oxide, which in turn is controlled by the powers applied on Si and SiO_2 targets [71]. This is illustrated in Fig. 1 which presents cross-section transmission electron microscopy (XTEM) and high resolution TEM (HRTEM) images of annealed SiO_x/SiO_2 multilayers. The Si QDs size increases when the concentration x decreases (QDs size of 2.2 – 2.5 nm for x =1.3, 3 – 3.5 nm for x =1 and 4 – 4.5 nm for x =0.86).

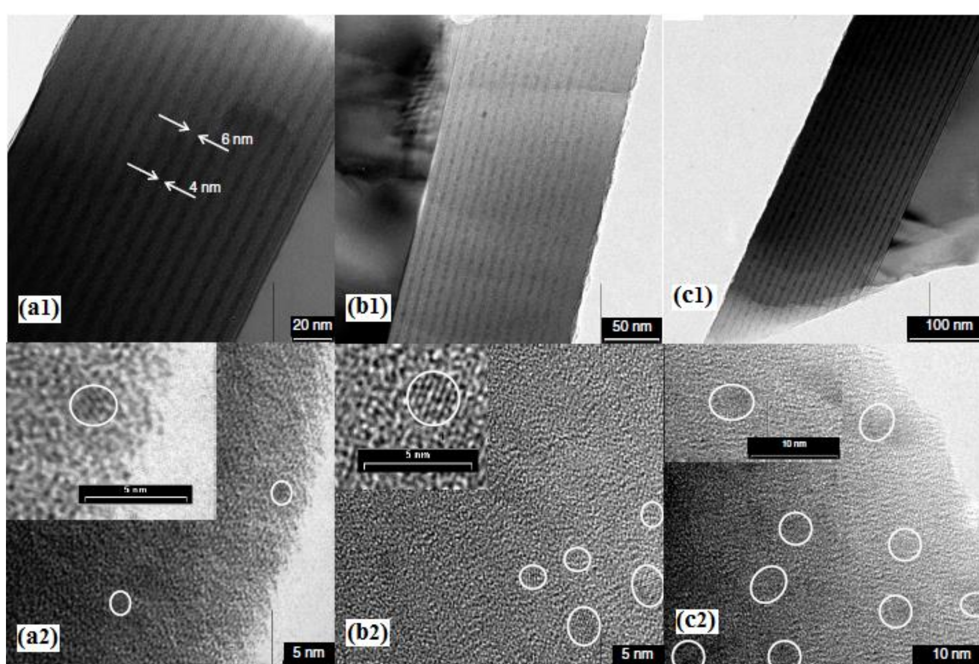

Fig. 1. *XTEM and HRTEM images taken on annealed SiO_x/SiO_2 multilayers: (a1) and (a2) $SiO_{1.30}$/SiO_2; (b1) and (b2) $SiO_{1.00}$/SiO_2; (c1) and (c2) $SiO_{0.86}$/SiO_2 [71]. (X. J. Hao, A. P. Podhorodecki, Y. S. Shen, G. Zatryb, J. Misiewicz and M. A. Green, "Effects of Si-rich oxide layer stoichiometry on the structural and optical properties of Si QD/SiO_2 multilayer films", Nanotechnology* ***20****, 485703 (2009),* http://dx.doi.org/10.1088/0957-4484/20/48/485703 . *© IOP Publishing. Reproduced by permission of IOP Publishing. All rights reserved)*

Gourbilleau [48] obtained similar structures as Hao [71], but the structures have been grown on heated substrate (500 °C) by using alternative reactive magnetron sputtering for Si-rich oxide layers and magnetron sputtering for SiO_2 layers. The Si incorporation in SiO_x ($x < 2$) was controlled by varying the H_2 partial pressure and substrate temperature.

The $Si_x(SiO_2)_{1-x}$ films co-sputtered on Si and quartz substrates at RT show after annealing different morphologies depending on x (Fig. 2) [49, 70, 73, 74, 99]. The films with low x (~10%) are practically amorphous, while in those with higher x (~ 20% or higher) (Fig. 2a), the Si NCs are formed and their diameters increase with the increase of Si concentration. In the case of 50% concentration of Si (Fig. 2b), the Si NCs form a network and for higher concentrations, the NCs with larger sizes contain nanotwin defects formed by the relaxation of stress produced by annealing (Fig. 2c).

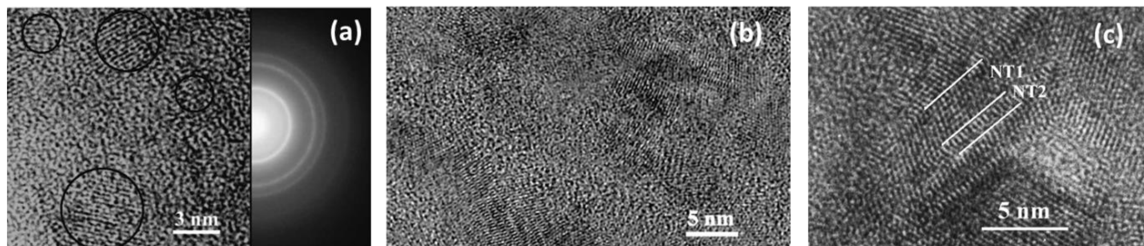

Fig. 2. *HRTEM images of annealed sputtered $Si_x(SiO_2)_{1-x}$ films with: (a) x ~ 20% including selected area electron diffraction (SAED) pattern (formation of NCs); (b) x ~ 50% (network of NCs); (c) x ~ 75% showing a large Si NC with nanotwins [49]. (Reprinted with permission from V. S. Teodorescu, M. L. Ciurea, V. Iancu, M.-G. Blanchin, Journal of Materials Research* ***23****, 2990 (2008), http://dx.doi.org/10.1557/JMR.2008.0358. Copyright 2008 Materials Research Society)*

2.1.2. Ion implantation

Ion implantation method is also used for obtaining Ge-SiO_2 and Si-SiO_2 films. For segregation of Ge or Si atoms and formation of NCs in SiO_2 matrix it is necessary an adequate annealing. Only a relatively small percent of excess Si crystallizes forming NCs [79]. Mokry *et al.* show the role of defects in the Si NCs formation. They observe a strong correlation between the position of Si NCs and their size distribution and the location of vacancies produced by implantation in SiO_2. During annealing, the defects heal and this leads to slowing the growth of Si NCs up to stopping it.

The parameters specific to implantation are the ions energy and dose which influence the NCs size and the depth profile of NCs volume fraction in SiO_2 [80]. By decreasing the implantation energy, the Si NCs size increases and the depth distribution of Si NCs narrows and shifts toward the films surface [55, 80]. The Si implantation process generates Si-rich type defects and oxygen-deficiency centres [54, 79].

In SiO_2 films implanted with Si ions at high-dose (and then annealed), the presence of perfect, extended and mismatch dislocations into big Si NCs (20 nm) was evidenced and they were correlated with the formation of Si NCs [78]. The perfect dislocations (Fig. 3) appear from the residual stress produced during Si NCs formation. The extended dislocations result by dissociation of a perfect dislocation, and the mismatch dislocations are produced by coalescence of two small NCs with different crystalline orientations.

In general, these SiO_2 films with embedded Si NCs obtained by implantation and subsequent annealing at 1000 – 1100 ^{o}C that are typical temperatures for Si-SiO_2 films present intense photoluminescence [54, 100].

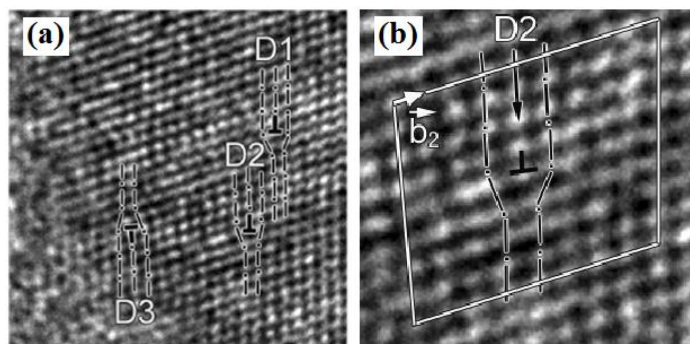

Fig. 3. *HRTEM image of a typical Si NC: (a) D1, D2, and D3 perfect dislocations and (b) Burgers circuit for D2 [78]. (Reprinted with permission from Y. Q. Wang, T. Li, W. S. Liang, X. F. Duan, G. G. Ross, "Dislocations in Si nanocrystals embedded in SiO_2", Nanotechnology* ***20****, 485703 (2009), http://dx.doi.org/10.1088/0957-4484/20/31/315704 . © IOP Publishing. Reproduced by permission of IOP Publishing. All rights reserved)*

Ge NCs in SiO_2 films were also obtained by Ge ions implantation and subsequent annealing [52, 53, 101]. Similarly to the case of Si, the ion dose influences the sizes and

distribution of Ge NCs [52], so that for doses smaller than a limit (10^{15} cm^{-2}), Ge NCs don't form [101]. At higher doses, the average size and concentration of Ge NCs increase, but by further increasing the dose, both decrease. The size change of Ge NCs with the increase of dose was correlated with the increase of the concentration of defects produced by implantation [101]. Additionally, Ge ions implantation produces (oxygen) vacancies [52] as in the case of Si. The implantation method gives the possibility to introduce the Ge ions with single or multiple energies [53], in the last case the size distribution of Ge NCs is more uniform.

2.1.3. Chemical vapour deposition

Plasma enhanced CVD represents another suitable method for obtaining Si NCs or QDs dispersed in SiO_2 films and in Si/SiO_2 or SiO_x/SiO_2 ($x < 2$) multilayers [57, 59, 81, 83]. In Ref. [57] it is demonstrated that in SiO_x/SiO_2 ($x < 2$) multilayers in which the layers are 2D systems, the size of Si QDs can be controlled by changing the SiO_2 layer thicknesses (through deposition time) as in the case of magnetron sputtering. So, by decreasing the SiO_2 thickness, Si QDs form and their size increases. Si QDs are surrounded by a thin suboxide (Si-rich oxide), and defects located at the QDs interface with matrix are present, which essentially contribute to the photoluminescence in the multilayers with big Si QDs [57, 59]. The density of localized states at interface is proportional to the fraction of oxygen-related bonds, which in turn increases with the increase of the Si NCs size [59].

An important parameter in the plasma enhanced CVD process is the flow ratio of working gases. Si-rich oxide films were deposited varying the ratio of flow rates of SiH_4 and N_2O precursors with the aim to control the Si content in the Si-rich oxide SiO_x ($x < 2$) [59].

Plasma enhanced CVD is also used for obtaining Ge NCs if the as-deposited films are subsequently annealed [30, 58, 81]. By varying the flux of the GeH_4 or SiH_4 precursors, Ge-SiO_2 films and multilayers with different Ge concentrations and controlled Ge NCs sizes were obtained [30]. If the substrate is heated (200 – 250 ^oC), the as-deposited films contain Ge or Si QDs, respectively [30, 57, 83].

The size and density of Ge QDs can be rigorously controlled by preparing metal-oxide-semiconductor (MOS) like structures depositing in the gate oxide poly-Si_xGe_{1-x} layers (1 or 3) separated from the substrate by a tunnellable dry Si oxide [102]. After ultrahigh vacuum CVD deposition, the structures were oxidized in H_2/O_2 at 900 ^oC, resulting Ge QDs with 9 nm size and ~10^{11} cm^{-2} spatial density for the case of one layer, and more packed QDs of ~10^{17} – 10^{18} cm^{-2} density having 5 nm size for the case of three layers.

A similar structure was prepared by replacing the tunnellable SiO_2 with Si_3N_4 [26]. Surprisingly, the Ge QDs are formed inside Si_3N_4 layer and their sizes are controlled by the thickness of Si_xGe_{1-x} layers, as seen in Fig. 4.

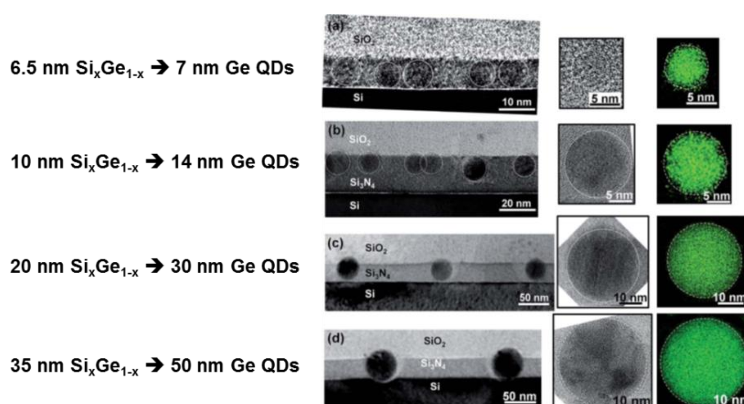

Fig. 4. *TEM images of MOS-like structures containing Ge QDs with different sizes dependent on the thickness of Si_xGe_{1-x} layers [26]. (C. Y. Chien, W. T. Lai, Y. J. Chang, C. C. Wang, M. H. Kuo, P. W. Li, Nanoscale **6**, 5303 (2014),* http://dx.doi.org/10.1039/C4NR00168K *. Reproduced by permission of The Royal Society of Chemistry)*

2.1.4. Sol-gel method

The sol-gel method followed by annealing is a fast process with a low cost that can be used for obtaining Ge NCs and amorphous NPs. Usually, the Ge-SiO_2 films prepared by this method present near the Si substrate a clear SiO_2 band (Fig. 5a) formed during films annealing, which is free of Ge NPs [29, 45, 61].

With the increase of Ge concentration (limited at a low value by the sol-gel method), the amorphous NPs size practically does not vary, but the NPs density does and for high Ge concentration, the coalescence of NPs is evidenced [45].

The structure of annealed sol-gel films was compared with the one of magnetron sputtered films having similar Ge concentration [60]. It was shown that in the sol-gel films, the amount of amorphous Ge is higher, the density of Ge NCs is much lower, the distance between NCs is also higher and the NCs are surrounded by boundary shells of GeO_x and SiO_x. For the formation of Ge NCs, the sol-gel films are usually annealed in forming gas [60, 61] or pure H_2 atmosphere [87, 88]. In Fig. 5b, the formation of globular Ge NCs is evidenced [87]. The Ge NCs are polycrystalline and faceted after annealing in forming gas at 900°C [61].

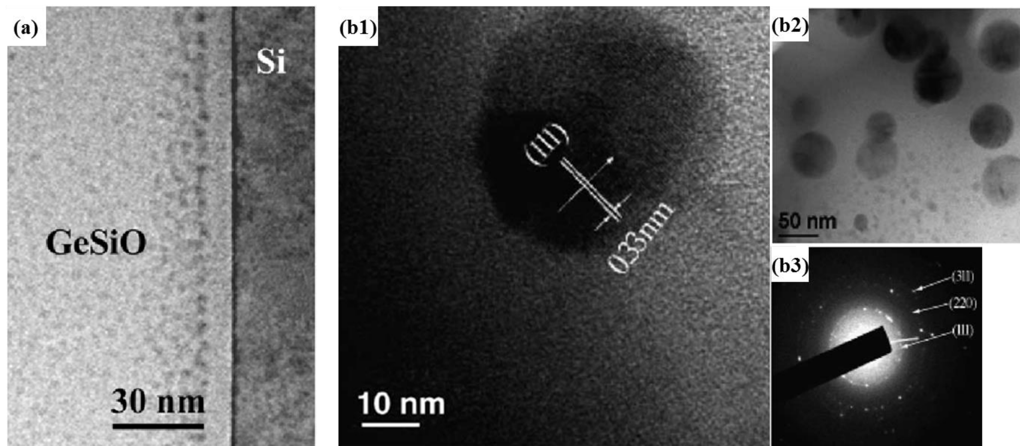

Fig. 5. *(a) XTEM image of a sol-gel Ge-SiO_2 film showing the film morphology at the interface with Si substrate [29] (Reprinted from Digest Journal of Nanomaterials and Biostructures* ***6*** *(1), pages 67-73 (2011), "Study of Ge nanoparticles embedded in an amorphous SiO_2 matrix with photoconductive properties", A. M. Lepadatu, I. Stavarache, T. F. Stoica, M. L. Ciurea, Copyright 2011, with permission from © Virtual Institute of Physics S.R.L.); (b) HRTEM images (b1 and b2) and SAED pattern (b3) obtained on sol-gel Ge-SiO_2 films annealed in H_2 (700°C, 30 min) showing the formation of Ge NCs [87] (Reprinted from Optical Materials, volume* ***27****, H. Yang, X. Yao, S. Xie, X. Wang, S. Liu, Y. Fang, X. Gu, F. Wang, Structure and photoluminescence of Ge nanoparticles embedded in SiO_2 gel glasses fabricated at different temperatures, pages 725–730, Copyright (2005), with permission from Elsevier).*

2.1.5. Molecular beam epitaxy

MBE method is seldom used compared with magnetron sputtering and ion implantation. It is used mainly for obtaining Ge NCs known as islands, grown on SiO_2. The NCs size and density are controlled by varying the substrate temperature during film growth [63] and also the thickness of the deposited Ge layer [92]. The increase of substrate temperature produces the NCs density decrease from highly packed to isolated NCs and the NCs diameter increase [63]. The increase of Ge layer thickness leads to the increase of both Ge NCs size and density [92]. The growth time of films influences the shape, size and density of NCs, so with the time increase, the small NCs suffer coalescence forming multifaceted dome-like NCs [64].

2.2. Changes produced by annealing on film structure and morphology

The as-deposited films grown on substrates maintained at RT are generally amorphous, independently on the used method in contrast to those deposited on heated substrates that contain

QDs or clusters. For NCs formation (nanostructuring) in the as-deposited amorphous films and for improving the morphology of films (the increase of QDs or clusters sizes) deposited on heated substrates, the annealing under controlled conditions is necesarry. The controlled parameters are the temperature, ramps of increasing/decreasing temperature, duration, atmosphere (N_2, H_2, Ar) [44, 47, 103, 104] and sometimes pressure [45, 105]. The annealing can be performed in conventional furnace (CF) or by rapid thermal annealing (RTA) [98, 103, 104], so that the morphology and structure of annealed films are dependent on the annealing conditions. Also for nanostructuring, other methods as the microwave annealing [106], laser annealing [82, 107] or ion-beam irradiation [108] are reported in literature.

The processes of segregation and diffusion of Ge or Si play an important role in the formation of NCs or NPs [44, 54, 86, 98]. Frequently, with the increase of annealing temperature the degree of Ge and Si crystallization increases together with the size of NCs [44, 47, 53, 59, 60, 75] as Raman spectroscopy and TEM show.

2.2.1. Films with Ge NCs/NPs in SiO_2

Ge NCs are formed by annealing at 600 – 1000 °C and are evidenced in Raman spectra by the presence of a peak, which is located at a position near the peak corresponding to bulk Ge (299.8 cm^{-1} [98]). This peak corresponding to Ge NCs is wider and asymmetric, and red- or blue-shifted in respect to the bulk Ge peak [52, 53]. The increase of the intensity of Ge NCs peak when the annealing temperature increases shows the increase of Ge crystallization degree [44, 47] as it is revealed in Fig. 6a. Annealing in CF at 700 °C in N_2 was shown to be favourable for obtaining films with fully crystallized Ge in NCs embedded in amorphous SiO_2 [44]. However, the annealing in CF is efficient for the Ge NCs formation up to 700 – 800 °C, only [44, 109]. In this temperature range, the segregation rate of Ge is higher than its diffusion rate. For annealing in CF at higher temperatures (800 – 1000 °C), the intensity of Raman peak corresponding to Ge NCs strongly decreases [44, 47, 110] (Fig. 6a) or even no Raman signal related to the amorphous or small clusters of Ge is evidenced. This is explained by the oxidation of Ge. In this case, the Ge diffusion is enhanced spreading the Ge atoms in the oxide matrix, hindering the Ge segregation that has a much smaller rate [98]. In Ref. [47] it is shown that the decrease of Raman signal is due to the decrease of NCs density and sizes (Fig. 6b and 6c). At high temperatures a part of Ge is lost as Ge oxide [61], as Rutherford backscattering spectrometry confirms [60]. This outdifussion of Ge was evidenced in TEM images by the presence of a zone either free of Ge near the free surface [61] or having a very low Ge concentration [47, 60] (Fig. 6c).

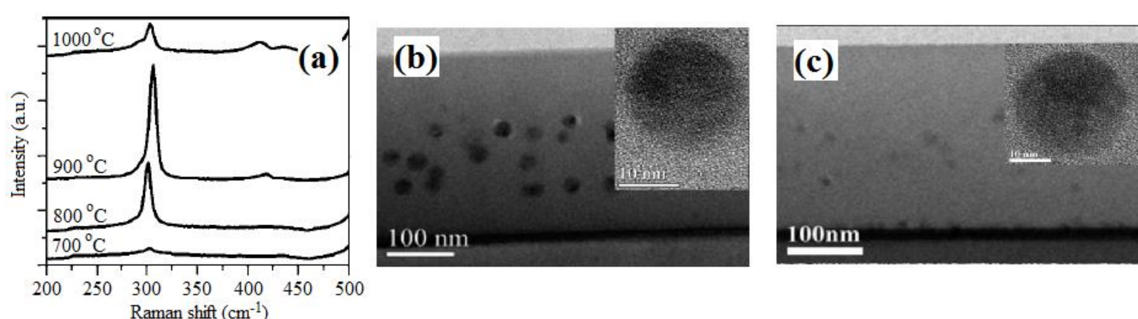

Fig. 6. *Ge-SiO$_2$ films annealed in forming gas for 15 min: (a) left - Raman spectra for 700 to 1000 °C annealing temperatures and right - XTEM images of films annealed at (b) 900 °C and (c) 1000 °C. HRTEM images in insets evidence Ge NCs [47]. (Reproduced with permission from W. K. Choi, H. G. Chew, F. Zheng, W. K. Chim, Y. L. Foo, E. A. Fitzgerald, Applied Physics Letters **89**, 113126 (2006), http://dx.doi.org/10.1063/1.2354012. Copyright 2006, AIP Publishing LLC)*

$[(Ge+SiO_2)/SiO_2]_{20}/Si$ multilayers annealed at different temperatures (belonging to five intervals) have different morphologies [108]. So, up to 300 °C no clusters are formed, weak clustering is observed between 300 and 550 °C, prominent clustering in the 550 – 750 °C range and strong clustering from 750 to 850 °C and for annealing temperature higher than 850 °C, the layered

structure is destroyed. It was shown that the nanostructuring can be also realized by irradiation of multilayers with Si or O ions. The five temperature intervals used for nanostructuring presented above were found again by adjusting the ion energies.

The competition between the processes of Ge segregation and diffusion was demonstrated by comparing the effect produced by annealing in CF with that produced by RTA on Ge/SiO_2 multilayered nanostructures [98]. So, in the case of nanostructures annealed in CF between 650 and 700 ^oC, amorphous Ge NPs are evidenced in the middle of SiO_2 layers as TEM images show, while Raman spectra show the presence of Ge NCs only in the 650 ^oC annealed nanostructures (Fig. 7). At higher temperature (800 ^oC) annealing, the Ge difussion is very strong, so that the multilayer aspect is destroyed. The drawback of the strong diffusion can be overcome by using RTA annealing that has been proved to be efficient in producing Ge NCs at fixed positions in multilayers annealed at all temperatures as is shown in Fig. 7 [98]. In the case of RTA, the initial multilayer aspect of nanostructures is maintained after RTA annealing at similar temperatures of 650, 700 and 800 ^oC as those used in CF. This means that the RTA annealing has the advantage to favour the Ge crystallization and to hinder the Ge diffusion. Other reports show that RTA in comparison with CF annealing produces a better crystallization of Si leading to the formation of Si NCs [104], but in other works no influence of the type of annealing (RTA or CF) was observed [94].

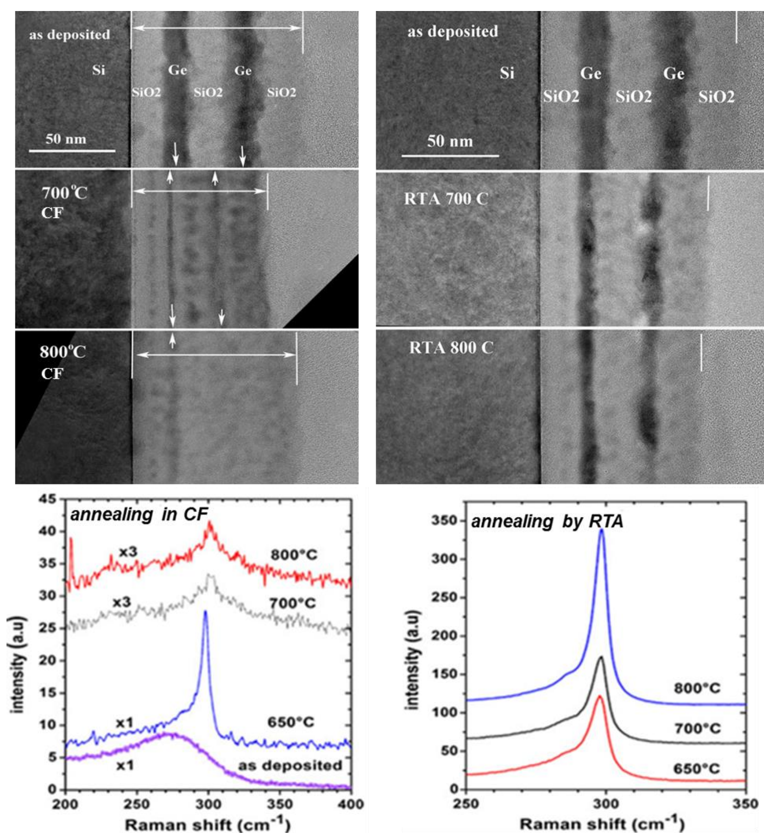

Fig. 7. *XTEM images and Raman spectra of Ge/SiO_2 multilayered nanostructures: as-deposited and annealed (650, 700 and 800 ^oC) in CF or by RTA [98]. (Reprinted with permission from Journal of Nanoparticle Research* ***15****, 1981 (2013), "Dense Ge nanocrystal layers embedded in oxide obtained by controlling the diffusion–crystallization process", A. M. Lepadatu, T. Stoica, I. Stavarache, V. S. Teodorescu, D. Buca, M. L. Ciurea. Copyright © 2013, Springer Science+Business Media Dordrecht)*

The annealing of sol-gel films at 800 – 950 ^oC in N_2 using RTA leads to the formation of Ge NPs that are mainly amorphous, but some NPs present in HRTEM images, traces of lattice fringes corresponding to the tetragonal Ge structure, which is a typical high pressure phase [29, 45]. Annealing processes in pure H_2 at relatively low temperatures (500 ^oC) [45] and in forming gas at temperatures from 600 to 900 ^oC [60] were also performed on the sol-gel films. In the films

annealed at low temperatures in pure H_2 Ge NCs are not formed, but amorphous Ge NPs. Some of NPs show traces of tetragonal structure [45]. The annealing at higher temperatures in forming gas leads to the formation of Ge NCs and the Ge NCs concentration is greatest in films annealed at highest temperature (900 ^oC) [60].

From the above, one can see that the atmosphere in which the samples are annealed influences the structure of films. The annealing of Ge-SiO_2 films with low Ge concentration in forming gas in CF leads to the formation of Ge NCs, while in N_2 atmosphere Ge NCs do not form (Raman spectroscopy) as H_2 reduces Ge oxides and increases the diffusivity of Ge atoms [47]. Other group [45, 105, 111] has found that the annealing in H_2 at 500 ^oC and 2 atm of Ge-SiO_2 sputtered films leads to the formation of big Ge NCs with Ge-III/ST12 tetragonal structure evidenced in Fig. 8a and having low density. Besides the big Ge NCs, the films contain a network of small amorphous NPs with high density. This double-morphology is the result of two mechanisms of Ge segregation [105]. On one hand, the segregation starts from the Ge nuclei due to the local fluctuation of Ge concentration. Then, these nuclei collect many Ge species forming big Ge NCs. This process produces local stress. On the other hand, the small amorphous NPs result from a uniform nucleation in the whole film volume. Also, big Ge NCs with tetragonal structure were found in the SiO_2/Ge/SiO_2 layers deposited by reactive magnetron sputtering on heated substrate at 400 ^oC [65]. The big tetragonal Ge NCs coexist with small cubic Ge NCs, as results from X-ray diffractograms. The tetragonal NCs are reported to be obtained using oxygen with high partial pressure during deposition. In this case, the roughness of the bottom SiO_2 layer increases and determines the increase of number of Ge nucleation centres. The tetragonal structure is a unusual phase for Ge NCs in SiO_2 matrix, usually the Ge NCs with cubic structure are reported in literature (see Fig. 8b) [68, 112].

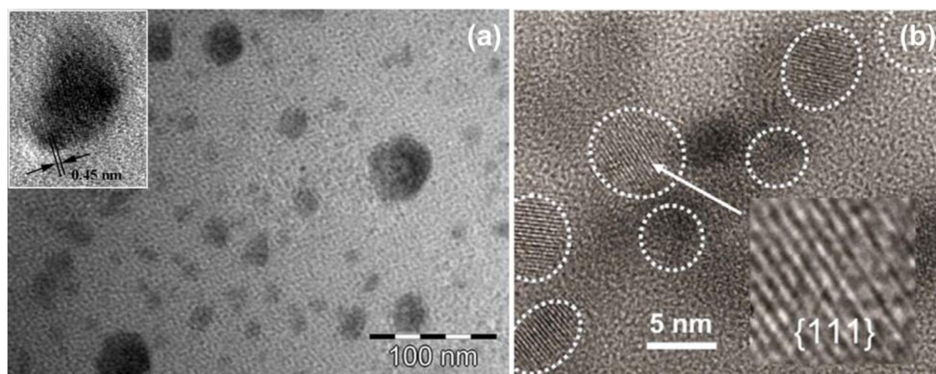

Fig. 8. *(a) XTEM image revealing the double-morphology of a Ge-SiO_2 sputtered film annealed in H_2 at 500 ^oC and 2 atm [111] (Reprinted with permission from Journal of Nanoparticle Research **14**, 930 (2012), "Structure and electrical transport in films of Ge nanoparticles embedded in SiO_2 matrix", I. Stavarache, A. M. Lepadatu, A. V. Maraloiu, V. S. Teodorescu, M. L. Ciurea. Copyright © 2012, Springer Science+Business Media B.V.). Inset: HRTEM image showing a 10 nm Ge NC with tetragonal structure (0.45 nm fringe spacing) [45] (Reprinted with permission from Journal of Nanoparticle Research **13**, 221–232 (2011), "Structural investigations of Ge nanoparticles embedded in an amorphous SiO_2 matrix", I. Stavarache, A. M. Lepadatu, N. G. Gheorghe, R. M. Costescu, G. E. Stan, D. Marcov, A. Slav, G. Iordache, T. F. Stoica, V. Iancu, V. S. Teodorescu, C. M. Teodorescu, M. L. Ciurea. Copyright © 2010, Springer Science+Business Media B.V.); (b) HRTEM image of a Ge-SiO_2 film deposited on heated substrate evidencing Ge NCs (encircled) with cubic structure (inset showing the lattice fringes of (111) lattice planes of cubic Ge) [112] (B. Zhang, Y. Yao, R. Patterson, S. Shrestha, M. A. Green, G. Conibeer, "Electrical properties of conductive Ge nanocrystal thin films fabricated by low temperature in situ growth", Nanotechnology **22**, 125204 (2011), http://dx.doi.org/10.1088/0957-4484/22/12/125204. © IOP Publishing. Reproduced by permission of IOP Publishing. All rights reserved).*

In sol-gel Ge-SiO_2 films annealed either in N_2 at high temperature (800 ^oC) or in H_2 at lower temperature (500 ^oC), no differences in structure and morphology were evidenced. These

films are formed mainly of amorphous Ge NPs embedded in SiO_2 matrix [45]. On contrary, in the sol-gel films annealed in Ar:CO or in Ar:H_2, Ge is crystallized forming Ge NCs with cubic structure [86].

The annealed films, independently on the method used for their deposition are stressed. A number of reports show the presence of the compressive stress in sputtered Ge-SiO_2 films that can be easily evidenced by the shift of Ge NCs Raman peak to higher energies [47] or can be seen in X-ray diffractograms [66]. The increase of stress is correlated with the increase of Ge crystallization degree and with the increase of Ge NCs size, as well [47]. The compressive stress was observed in sol-gel films, too, which presence is correlated with the formation of GeO_x or SiO_x boundary shells that cover the Ge NCs and form the interface with the SiO_2 matrix [60]. In the multilayered structures deposited by magnetron sputtering on heated substrate (360 ^oC), the compressive stress is present even in the as-deposited structures [66] that partially relaxes by subsequent annealing. In this case, the stress is also correlated with a core-shell structure in which Ge NCs (cores) are covered by an amorphous Ge-rich shell.

In the films with Ge NCs in SiO_2 obtained by Ge ions implantation and further annealing, besides the compressive stress, defects inside the Ge NCs were observed [75]. The most evidenced defects are twinning and stacking faults (planar defects) and dislocations (linear ones) (Fig. 9). The concentrations of these defects were found to vary in a different way with the increase of annealing temperature. Particularly, the concentration of dislocations is correlated with the intensity of the stress field (evaluated from the variation of interplanar spaces), meaning that the concentration of dislocations has similar dependence on the annealing temperature as the stress field intensity. The dislocations concentration reaches its maximum together with the stress field intensity in the films annealed at 1100 ^oC.

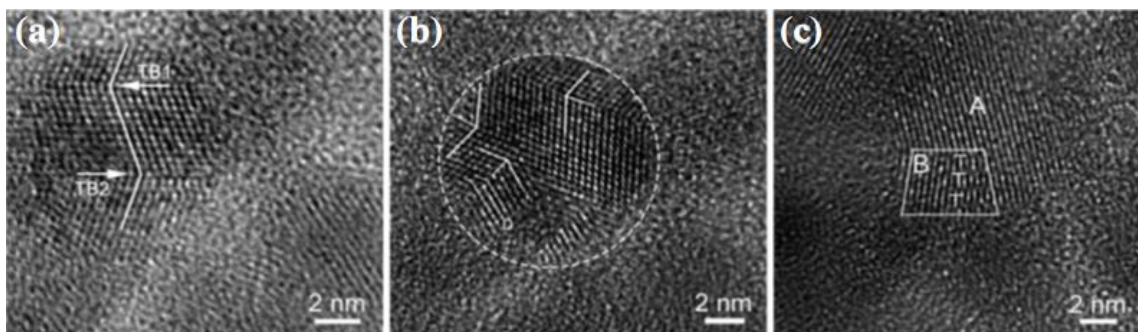

Fig. 9. *HRTEM images of a Ge-SiO_2 film obtained by implantation and annealing at 850 °C evidencing: (a) a Ge NC with nanotwins (TB1 and TB2 twin boundaries); (b) NCs with different orientations about to connect and a dislocation (D) near a twin boundary; (c) NCs A and B with different orientations and three dislocations (T) present at the interface between NCs A and B [75]. (Reprinted from Materials Characterization, volume* ***93****, M. Zhang, R. Cai, Y. Zhang, C. Wang, Y. Wang, G. G. Ross, D. Barba, Evolution of microstructural defects with strain effects in germanium nanocrystals synthesized at different annealing temperatures, pages 1–9, Copyright (2014), with permission from Elsevier)*

2.2.2. Films with Si NCs/NPs in SiO_2

In the case of Si-SiO_2 films or multilayers deposited by magnetron sputtering and annealed in CF, the most efficient annealing temperatures for obtaining Si NCs are in the range of 1000 – 1200 ^oC [48, 49, 70–72]. For example, 1100 ^oC is the optimum temperature for obtaining Si nanoclusters in SiO_x (x<2) / SiO_2 multilayers [48]. After annealing of these structures, the defects are healed and the photoluminescence emission from Si NCs becomes optimum. Using Raman spectroscopy, Si NCs are evidenced by the peak corresponding to the transverse optical mode of phonons in Si NCs, located close to the bulk Si position (520 cm^{-1}) [57, 91]. This peak is wider and slightly asymmetric than the one corresponding to bulk Si as one can see in Fig. 10. The less intense broad maxima located around 150, 300, 380, and 480 cm^{-1} correspond to different phonon modes in amorphous Si [59]. With the increase of annealing temperature, the crystallization is

enhanced, being demonstrated by the increase of intensity of Si NCs peak together with the strong decrease of amorphous Raman contribution (Fig. 10) [59]. Additionally, with the increase of the annealing temperature, the size of Si NCs increases and therefore it can be controlled [48, 50].

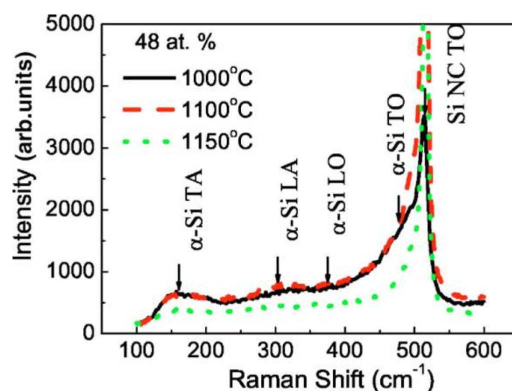

Fig. 10. *Raman spectra measured on Si-rich oxide films annealed at 1000 °C, 1100 °C, and 1150 °C for 1 h in N_2 [59]. (Reprinted figure with permission from X. X. Wang, J. G. Zhang, L. Ding, B. W. Cheng, W. K. Ge, J. Z. Yu, Q. M. Wang, Physical Review B* ***72****, 195313 (2005), http://journals.aps.org/prb/abstract/10.1103/PhysRevB.72.195313. Copyright (2005) by the American Physical Society)*

Annealing of Si-SiO_2 films or multilayers can be made either by RTA or in CF (as above) [54, 83, 94]. No influence of the type of annealing was observed on the formation and size of Si NCs in SiO_x/SiO_2 multilayers. These nanostructures contain a high density of defects located at the interface between NC and matrix, being higher in the RTA annealed multilayers [94]. To diminish the defects density, a postannealing passivation in H_2 was performed, which is more efficient in CF annealed structures.

The annealing is usually performed in N_2 and Ar atmospheres. For example, by annealing Si-rich oxide/SiO_2 multilayered structures in N_2, Si NCs with small size and low density are obtained in contrast with the case of annealing in Ar when bigger NCs with higher density are observed [56]. The effect of annealing in N_2 on Si NCs formation is explained by the suppression of Si diffusion produced by the presence of N_2. The annealing in N_2 leads to the decrease of fraction of Si=O bonds, but Si-N bonds form by incorporating N in the shell of Si NCs [59]. These films have strong photoluminescence emission explained by quantum confinement in Si NCs.

Similarly to the case of Ge-SiO_2, in Si-SiO_2 films and structures containing Si NCs, the presence of stress field and defects should be considered [113, 114]. In Si-SiO_2 films with high concentration of Si NCs having diameters higher than 10 nm, nanotwins (Fig. 2c) and stacking faults were observed [49]. They are formed by the partial relaxation of the local stress field present in the films. Twin boundaries were evidenced within Si NCs [48]. Zatryb et al. [115] produced compressive stress in Si NCs by varying the partial pressure of H_2 during reactive sputtering deposition. The authors observed that with the increase of H_2 partial pressure, the order degree of oxide matrix increases (FTIR) together with the compressive stress (Raman).

3. Electrical and photoconductive properties of structures formed of Ge or Si NCs or NPs embedded in SiO_2

The films with Ge or Si NCs/NPs in SiO_2 are percolative systems, therefore the electrical transport takes place either by hopping or tunnelling mechanisms.

3.1. Films with Ge NCs/NPs in SiO_2

In Ge-SiO_2 films (3 – 5 μm thick) formed of Ge NCs randomly distributed in amorphous SiO_2 and separated to each other by few nm, the thermally activated tunnelling of carriers between neighbouring Ge NCs was evidenced [68]. The conductivity-temperature ($\sigma - T$) characteristics

measured on films with different concentrations of Ge NCs have been shown that the conductivity depends on temperature according to the formula $\sigma = A\exp\left[-(T_0/T)^{1/2}\right]$ (Fig. 11), in which A is a constant and T_0 is the characteristic temperature. T_0 is given by the expression $T_0 = (2P_c s_{\max} E_{a,\max})/(k_B a)$, being dependent on the percolation threshold P_c which in its turn depends on the concentration of percolation sites. Also, T_0 depends on the maximum separation distance s_{max} between nearest NCs, on the maximum activation energy $E_{a,\max}$ and on the decay length a of the wave function. The authors consider the system of Ge NCs embedded in amorphous SiO_2 as a 3D network of Ge NCs that play the role of sites that are connected to the neighbouring NCs by finite tunnelling "resistances" (in the percolation theory). The finite "resistances" actually are tunnelling barriers given by the thin SiO_2 layers (s_{max} being 3 nm) between NCs. The charge transport is ensured by the carriers that tunnel barriers between the nearest-neighbour NCs. The activation energy necessary for this process is the sum of the electrostatic charging energy of NC and the energy difference corresponding to the shift of the conduction band edge in respect to the bulk one. This energy difference is due to the quantum confinement effect. Actually, $E_{a,\max}$ represents the maximum activation energy corresponding to the tunnelling from the biggest to the smallest NCs. T_0 was evaluated by calculating $E_{a,max}$ knowing P_c = 0.25 for a cubic lattice of sites and a = 1 nm. The characteristic temperature was experimentally determined and was found to decrease with the increase of Ge NCs concentration. As an example, by increasing the concentration from 4.2% to 15.3%, the diameter increases from 3.8 to 8.9 nm, and T_0 decreases from about 2×10^5 to 1×10^5 K. For all films (with different thickness and with different concentration of Ge NCs), σ is almost independent on the voltage increase, and increases by four orders of magnitude with the increase of Ge NCs concentration from 4.2% to 15.3%.

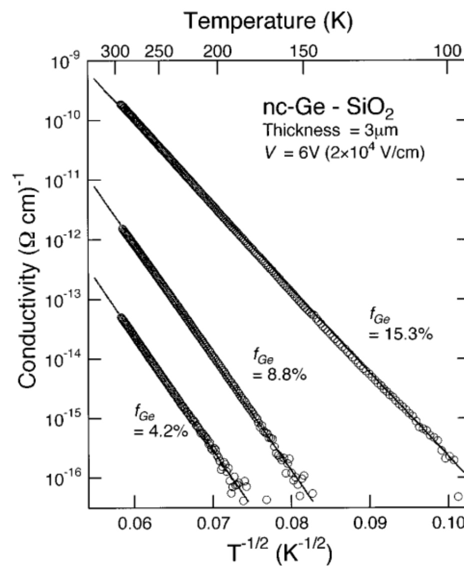

Fig. 11. *$\sigma - T$ characteristics measured on Ge-SiO_2 films with different Ge NCs concentrations of 4.2%, 8.8% and 15.3%:* $\sigma = A\exp\left[-(T_0/T)^{1/2}\right]$ *dependence [68].*
(Reprinted with permission from M. Fujii, O. Mamezaki, S. Hayashi, K. Yamamoto, Journal of Applied Physics ***83****, 1507 (1998), http://dx.doi.org/10.1063/1.366858.*
Copyright 1998, AIP Publishing LLC)

In contrast, the Mott variable range-hopping was found in Ge-SiO_2 films of 200 nm thickness, containing Ge clusters dispersed in SiO_x matrix. This process takes place through localized states associated with clusters [116]. The measured $\sigma - T$ characteristics show a dependence of conductivity on temperature following the $\ln\sigma \propto T^{-1/4}$ law from about 100 to 300 K. In accordance with the Mott model $\sigma = B\exp\left[-(T_0/T)^{1/4}\right]$, B is a constant and the characteristic

temperature T_0 is given by the formula $T_0 = 2.06a^3 k_B N(E_f)$ in which a is the decay length of the wave function of localized states and $N(E_f)$ is the density of states at Fermi energy.

In Ref. [44], the tunability of electrical properties through the variation of the annealing conditions was demonstrated. In Ge-SiO_2 films with atomic ratio of Ge/Si=1.9 and 200 nm thickness, the transport mechanism is governed either by tunnelling or hopping in function of annealing temperature. So, the electrical behaviour of films formed of Ge NCs (12 nm) embedded in amorphous SiO_2 after 700 °C annealing was compared with the behaviour of films containing small disordered Ge clusters obtained for 800 °C annealing. The current-voltage (I – V) dependence measured on Al/Ge-SiO_2/Si/Al diodes shows a rectifying behaviour for both types of films, mainly due to Al contacts on backside of Si wafers. The temperature dependence of the current (I – T) was measured by biasing the samples with a voltage higher than a voltage threshold from where the film contribution to the current is dominant in respect of the contribution of contacts.

In the films formed of Ge NCs in SiO_2 (700 °C annealing) it was shown that the current versus temperature has a $I \propto \exp\left[-(T_0/T)^{1/2}\right]$ dependence with $T_0 = 2.4 \times 10^5$ K (Fig. 12). This is to be expected for the system of Ge NCs embedded in amorphous SiO_2, the $\exp(T^{-1/2})$ behaviour being the signature of the mechanism of thermally activated tunnelling between neighbouring Ge NCs [117]. In contrast, the I – T characteristic measured on the films containing only small disordered Ge clusters (800 °C annealing), shows a $I \propto \exp\left[-(T_0/T)^{1/4}\right]$ dependence with T_0 having the value of 1.6×10^8 K (Fig. 12). In the last case, the authors of Ref. [44] considered the Pollak model as the best one for explaining the $\ln I \propto T^{-1/4}$ behaviour observable up to RT, which cannot be explained by the Mott model of variable range hopping. According to the Pollak model, the carriers hop between localized states which form a band of $2E_0$ width (0.36 eV) that is located near Fermi energy. The total concentration of localized states N can be estimated from the formula:

$$N = \int_{-E_0}^{E_0} g_0\left[1 - (E/E_0)^2\right] dE,$$

where the density of states at the Fermi level g_0 can be derived from the expression of the characteristic temperature $T_0 = \left(C^4 / k_B g_0 a^3\right)$ in which the constant C = 1.84 corresponds to amorphous Ge. The total concentration of localized states from the 0.36 eV-wide band was found to be about 2×10^{17} cm^{-3}. In these films the localized states are related to the small disorder Ge clusters Ge produced by the diffusion of Ge in SiO_2 after annealing.

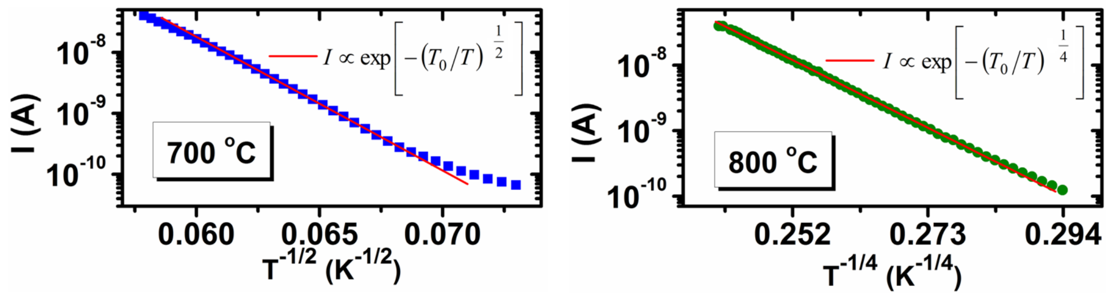

Fig. 12. *$I - T$ characteristics measured on Ge-SiO_2 films: $I \propto \exp\left[-(T_0/T)^{1/2}\right]$ dependence for 700 °C annealed films (Ge NCs in SiO_2) and $I \propto \exp\left[-(T_0/T)^{1/4}\right]$ dependence for 800 °C annealed films (small disordered Ge clusters) [44]. (Reprinted from Applied Surface Science, volume **285**(B), I. Stavarache, A. M. Lepadatu, T. Stoica, M. L. Ciurea, Annealing temperature effect on structure and electrical properties of films formed of Ge nanoparticles in SiO_2, pages 175–179, Copyright (2013), with permission from Elsevier)*

Similar $T^{-1/4}$ behaviour was evidenced in thicker Ge-SiO_2 films (2.5 μm) having a lower Ge concentration (atomic ratio Ge/Si=0.73) [111]. In these films, the preparation conditions

(deposition and especially annealing) lead to the formation of big tetragonal Ge NCs having low density and of a network of small amorphous NPs with high density, all NCs and amorphous NPs being embedded in SiO_2. The $I - T$ characteristics measured at different biases have two dependences, one at rather low temperatures (up to RT) and the other one at higher temperatures (Fig. 13) [111, 118]. At low temperatures, the current behaves on the temperature as $I \propto \exp\left[-(T_0/T)^{1/4}\right]$ with T_0 = 2.2 × 10^9 K, while at higher temperatures, the current has an Arrhenius dependence with an activation energy of 0.34 eV. These results are well correlated with the structure of films. The $T^{-1/4}$ behaviour at low temperatures is also explained by the Pollak model, in this case the band of localized states with concentration of 1.5 × 10^{16} cm^{-3} is related to the uniform network of small amorphous Ge NPs. On the other hand, at high temperatures the activated conductivity to extended states was found. The contribution of big NCs (few in the film) to the electrical transport is negligible. Conductivity-voltage ($\sigma - V$) characteristics were measured at low and high temperatures at which $T^{-1/4}$ and 1000/T behaviours were found and it was shown that σ practically does not vary with the voltage.

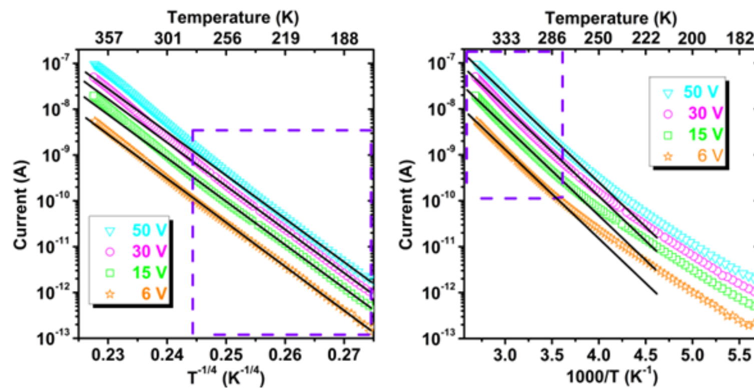

*Fig. 13. $I - T$ characteristics measured at biases of 6, 15, 30 and 50 V on Ge-SiO_2 films formed of low density big tetragonal Ge NCs and a network of high density small amorphous NPs: (left) lgI = f($T^{-1/4}$) representation and (right) lgI = f(1000/T) representation [111]. (Reprinted with permission from Journal of Nanoparticle Research **14**, 930 (2012), "Structure and electrical transport in films of Ge nanoparticles embedded in SiO_2 matrix", I. Stavarache, A. M. Lepadatu, A. V. Maraloiu, V. S. Teodorescu, M. L. Ciurea. Copyright © 2012, Springer Science+Business Media B.V.)*

As it can be seen from the above, in a system with small amorphous Ge NPs or disordered Ge clusters randomly distributed in the oxide, the electrical transport mechanism is essentially the same, namely Pollak hopping in a band of localized states near Fermi energy. In the case of films with smaller Ge concentration, the characteristic temperature T_0 is one order of magnitude higher than in the films with higher Ge concentration, while the total concentration of localized states N is one order of magnitude smaller. Interestingly, a similar exp($T^{-1/4}$) behaviour with a much higher T_0 (2.0 × 10^{10} K) was observed in films (250 – 280 nm thickness) prepared by sol-gel method that have a much lower Ge concentration than the other films discussed above [29]. These films contain only amorphous Ge NPs with a high density. By considering again the Pollak model with the same values for C and $2E_0$, the authors find a much smaller total concentration of localized states (1.6 × 10^{15} cm^{-3}) which correlates very well with the low Ge concentration in the sol-gel films.

In SiO_2/Ge/SiO_2/Si multilayers containing Ge NCs with cubic and tetragonal structure, different types of hopping mechanisms were evidenced by measuring resistivity-temperature ($\rho - T$) characteristics. The thickness of layers was controlled by the deposition time of 15 min for SiO_2 layers and 2 min for Ge layers. The $\rho - T$ characteristics show different temperature dependences [65], so that, at 35 – 60 K, three dimensional Mott variable range hopping was observed, while at higher temperatures of 60 – 160 K bidimensional Mott variable range hopping ($\ln\rho \propto T^{1/3}$) was found. As it was mentioned in Sections 2.1 and 2.2 the formation of Ge NCs is strongly influenced by the oxygen partial pressure during reactive sputtering that determines the roughness of SiO_2.

For low roughness, small NCs are formed and (three- and bidimensional) Mott variable range hopping mechanism was identified, while for high roughness, big Ge NCs are observed that are responsible for Efros-Shkovskii hopping mechanism.

A mechanism of thermally activated hopping was shown to take place between nearest neighbouring NCs in films of Ge NCs embedded in SiO_2 matrix [112]. The films of 250 – 300 nm thickness sputtered on heated quartz substrates contain Ge NCs with sizes between 3.8 and 8 nm, separated by distances of 1.5 – 4.5 nm. Hall measurements showed that holes are responsible for electrical conduction, their concentration being high of 3.2×10^{18} cm^{-3}. The holes are induced by the acceptor-like surface states related to dangling bonds and present in a 1 nm shell layer around NCs. The electrical properties of the as-deposited films were improved by a subsequent annealing (RTA), meaning that the conductivity of RTA films increases with almost three orders of magnitude than the one of as-deposited films (Fig. 14). This happens despite of the fact that the annealing produces minor changes in the film structure (the stoichiometry of matrix improves from SiO_x to SiO_2 and the holes accumulate in Ge NCs due to enhancement of dangling bonds produced by Ge-O bonds decomposition). The $I - V$ characteristics are linear for both as-deposited and annealed films and the conductivity increases with the annealing temperature increase. The $\sigma - T$ curves for both films have an Arrhenius dependence with one activation energy. This behaviour is explained by hopping of carriers from a NC to the states from nearest neighbouring NC by overcoming the electrostatic charging energy. The activation energy is also dependent on the annealing temperature and decreases from about 0.2 to 0.1 eV with the increase of annealing temperature from 650 to 800 ^{o}C, while for the as-deposited films its value is about 0.3 eV (Fig. 14).

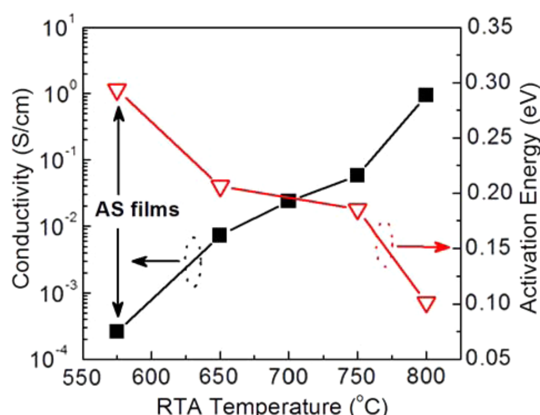

Fig. 14. *As-deposited (AS) and annealed Ge-SiO_2 films formed of Ge NCs embedded in SiO_2 matrix: conductivities and activation energies plotted in function of RTA temperatures [112] (B. Zhang, Y. Yao, R. Patterson, S. Shrestha, M. A. Green, G. Conibeer, "Electrical properties of conductive Ge nanocrystal thin films fabricated by low temperature in situ growth", Nanotechnology* ***22****, 125204 (2011),* *http://dx.doi.org/10.1088/0957-4484/22/12/125204. © IOP Publishing. Reproduced by permission of IOP Publishing. All rights reserved).*

In thin Ge-SiO_2 films (14 and 27 nm thickness) formed of Ge NCs in SiO_2, the $I - V$ characteristics measured at low temperatures (5 – 77 K) on samples with up-down geometry of contacts present nonperiodical "step-like structures" [119] (voltage intervals in which the current is practically constant). These "step-like structures" are dependent on the film thickness and are explained by the interplay between resonant tunnelling through discrete quantum confinement energy levels in the NCs and single electron charging effect of Ge NCs. The "step-like structure" appears as a result of carriers transport through the lowest resistance path, which probably contains the biggest NC (12 or 25 nm in thin or thicker films, respectively). The width of steps decreases with the increase of the NCs size, and it was shown to have almost similar values with the differences (divided by the electron charge e) between the energies of consecutive discrete energy states in Ge NCs.

The metal-insulator-semiconductor (MIS) structures using as insulator Ge-SiO_2 films present high photoconductive properties (400 – 1000 nm wavelength) either when Ge-SiO_2 films

are as-deposited (on heated substrate) or when they are annealed at 800 ^oC [27, 120]. The as-deposited films (~250 nm thick) contain densely packed amorphous Ge NPs (2 nm size and $2x10^{19}$ cm^{-3} density), while in the annealed films, more dispersed big Ge NCs (8 nm size and $6x10^{17}$ cm^{-3} density) are formed [27]. The $I - V$ characteristics measured in reverse bias in dark and under illumination are given in Fig. 15. Under illumination with monochromatic light, the reverse current increases with two orders of magnitude in respect to the dark current. The good photoconductive properties of MIS devices are explained by the trapping of photogenerated holes at Ge NCs or NPs interface states, which produces the supplementary injection of electrons (from IZO contact) enhancing the photocurrent. The spectral responsivity was calculated for low and high reverse biases and it was found that the curves are very broad as it is shown in Fig. 15. At high bias, the responsivity is very high (4 A/W) for both as-deposited and annealed films, but the maxima are located at different positions due to increase of the NCs size after annealing and films densification, as well. The internal quantum efficiency was found to be high (700% – 800%) and practically independent on annealing because the optical gap is fixed by the interface states at the value of 1.6 eV.

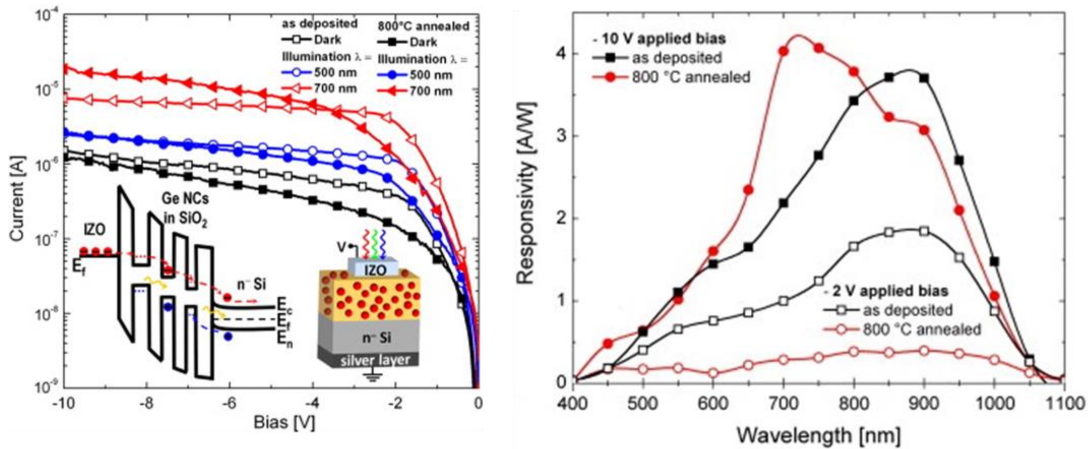

Fig. 15. *Left: dark current and photocurrent curves versus reverse biases taken on MIS structures containing as-deposited Ge-SiO_2 films and annealed ones; Right: spectral responsivities for both as-deposited and annealed films [27]. (Reprinted from Thin Solid Films, volume* ***548****, S. Cosentino, S. Mirabella, P. Liu, S. T. Le, M. Miritello, S. Lee, I. Crupi, G. Nicotra, C. Spinella, D. Paine, A. Terrasi, A. Zaslavsky, D. Pacifici, Role of Ge nanoclusters in the performance of photodetectors compatible with Si technology, pages 551–555, Copyright (2013), with permission from Elsevier)*

The MOS-like structures prepared by ultrahigh vacuum CVD and oxidized at 900 ^oC, containing stacks (1 or 3) of Ge QDs into the gate Si oxide present very high photoconductivity, the photocurrent being with 3 – 4 orders of magnitude higher than the dark current [102]. In these MOS diodes the transport mechanism in dark is the thermally activated tunnelling between neighbouring Ge QDs as it is demonstrated by the exp($T^{-1/2}$) dependence of the conductance $G \propto \exp\left[-\left(T_0/T\right)^{1/2}\right]$. The high photoconductivity and spectral photoresponsivity are explained by the quantum confinement effect in Ge QDs. The MOS devices obtained by replacing the tunnellable SiO_2 with Si_3N_4 present better photoconductive properties, the photocurrent being with at least four orders of magnitude higher than the dark current from ultraviolet to near infrared (300 – 1500 nm) [26]. The main contributions to the enhanced photoconductive properties are the quantum confinement effect (for small QDs) and the tensile strain that makes the indirect band gap of big NCs to become direct band gap.

Sol-gel films mainly formed of amorphous Ge NPs embedded in SiO_2 also present good photoconductive properties [29]. Some NPs present traces of lattice fringes corresponding to tetragonal structure as HRTEM images reveal, which suggests the presence of tetragonal clusters. The photocurrent has a broad spectral distribution between 350 and 900 nm with one maximum at 513 nm, two shoulders at 405 and 460 nm, and a narrow peak (full width at half maximum of few tenths of nm) positioned at 862 nm. The photocurrent-voltage (I_f – V) curves show good

photoresponse at both maxima (513 and 862 nm), the photocurrent being higher with at least two orders of magnitude than the dark current (Fig. 16). The structure of the spectral distribution curves is explained by considering both contributions of tetragonal clusters and localized states produced by RTA at the interface of NPs with matrix. The enhanced photocurrent is explained by the increase of the lifetime of free carriers by trapping the opposite sign ones.

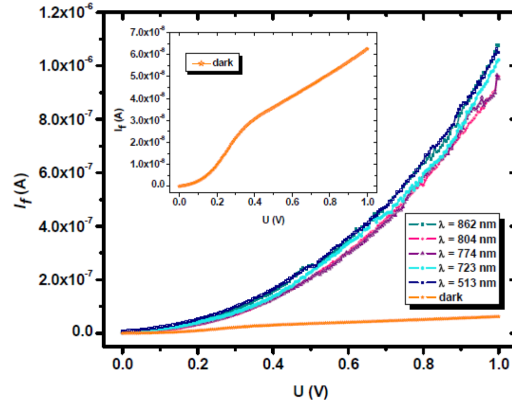

Fig. 16. *I_f – V characteristics obtained on sol-gel films mainly formed of Ge NPs embedded in SiO_2, but containing also some tetragonal clusters [29]. Also, for comparison is included the dark I – V curve. (Reprinted from Digest Journal of Nanomaterials and Biostructures* ***6*** *(1), pages 67-73 (2011), "Study of Ge nanoparticles embedded in an amorphous SiO_2 matrix with photoconductive properties", A. M. Lepadatu, I. Stavarache, T. F. Stoica, M. L. Ciurea, Copyright 2011, with permission from © Virtual Institute of Physics S.R.L.)*

3.2. Films with Si NCs/NPs in SiO_2

The electronic transport in Si NCs based films and multilayers is dependent on thickness and morphology of films, which in their turn depend on the preparation methods and parameters. So, the nanocrystalline Si films with thickness less than 10 nm are formed of Si NCs separated to each other by amorphous Si grain boundaries, the films with intermediate thickness (tens of nm) consist of nanochains of Si NCs (10 – 30 nm diameter) separated by SiO_2 necks with similar sizes or less, and the thick films (hundreds of nm) are formed of discrete Si NCs covered by SiO_2 shell [121]. In the nanocrystalline Si films thinner than 10 nm, an Arrhenius dependence of conductivity σ on temperature T, $\ln\sigma \propto 1/T$ was observed. This was explained by thermionic emission over potential barriers formed by amorphous Si grain boundaries. The measured activation energy from the $\ln\sigma \propto 1/T$ plot is given by the height of these potential barriers. If the NCs are small, the quantum confinement effect is strong, and therefore, single-electron charging takes place. In the case of nanochains of Si NCs separated by SiO_2 necks, I – V curves measured in an up-down geometry, at RT present multiple step Coulomb staircases explained by single electron charge effects.

In thick films formed of Si NCs (8 nm) with SiO_2 shells of 1.5 nm the transport is described at high temperature (200 – 300 K) by the space charge limited currents in the presence of trapping states with exponential distribution, while at low temperature by thermally activated tunnelling between adjacent NCs [122, 123]. The authors measured I – V curves (in up-down geometry) at different temperatures and found a power law dependence of current on voltage $I \propto V^m$, the exponent m linearly increasing with the reverse of temperature $1/T$ from 1.8 to 4 in the 300 – 200 K range. This is explained by injection of free carriers from the substrate/contact in the conduction states of NCs, part of them being trapped. By increasing the voltage, the Fermi level crosses the traps distribution, so that the concentration of free carriers rapidly increases.

At lower temperatures less than 200 K, the conductivity depends on temperature following the $\sigma = A\exp\left[-(T_0/T)^{1/2}\right]$ law (with A constant, T_0 characteristic temperature

$T_0 = (2P_c s_{max} E_{a,max})/(k_B a)$, P_c percolation threshold, s_{max} maximum separation distance between nearest NCs, $E_{a,max}$ maximum activation energy, and a decay length of the wave function), which is explained by thermally activated tunnelling between adjacent NCs in the frame of the percolation-hopping transport model [122]. The validity of the model was checked by comparing the characteristic temperature calculated from the model with the one determined from experiment, they being in good agreement. By varying the Si NCs sizes from 8 to 6 and 11 nm, the authors showed that T_0 decreases with the increase of NCs size (Fig. 17) [124].

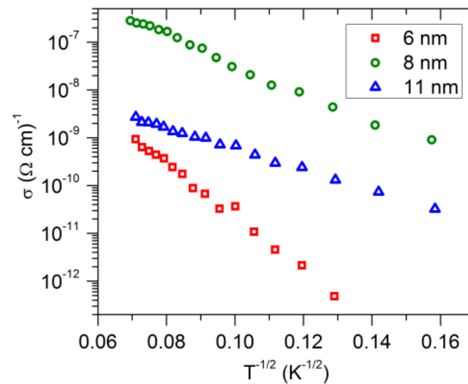

Fig. 17. $\ln\sigma \propto T^{-1/2}$ *curves measured on films formed of Si NCs (6, 8, and 11 nm) covered by SiO_2 shells [124]. (Reprinted and adapted from X. Zhou, K. Usami, M. A. Rafiq, Y. Tsuchiya, H. Mizuta, S. Oda, Journal of Applied Physics* ***104****, 024518 (2008), http://dx.doi.org/10.1063/1.2952036. Copyright 2008, AIP Publishing LLC)*

The SiO_2 films with embedded Si NCs obtained by Si-implantation present different behaviours of $I-V$ characteristics taken in up to down geometry contacts [55]. The shape of $I-V$ curves reflects different transport mechanisms on different voltage intervals and it is dependent on the distribution of Si NCs (Fig. 18a and 18b). Therefore, the observed transport mechanisms are the Fowler-Nordheim tunnelling from Si substrate to SiO_2 matrix, Frenkel-Poole emission and NCs-assisted tunneling. In films with narrow depth distribution of Si NCs located close to the free surface of films, the electrical behaviour is similar to the one of a SiO_2 layer of similar thickness, but showing a lower onset voltage of Fowler-Nordheim tunnelling of electrons from substrate into the oxide. In the films with wider depth distribution, the conduction mechanisms related to NCs become important and many percolative paths are present. The percolative character is demonstrated by the power law behaviour of $I-V$ characteristic.

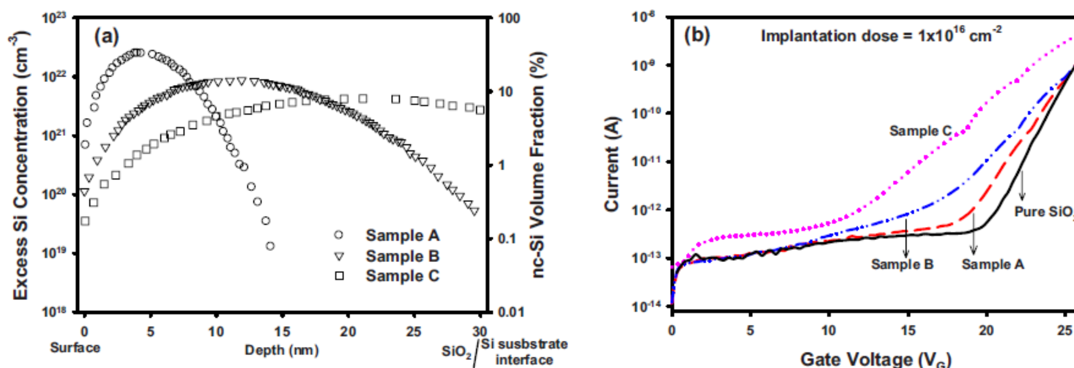

Fig. 18. *(a) Different Si NC distributions in the SiO_2 implanted films, resulted from SRIM simulation: Sample A - narrow depth distribution close to the films surface, Samples B and C - wider depth distribution; (b) $I-V$ characteristics taken on samples A, B, and C and on a pure SiO_2 [55]. (Reprinted and adapted from J. I. Wong, T. P. Chen, M. Yang, Y. Liu, C. Y. Ng, L. Ding, Journal of Applied Physics* ***106****, 013718 (2009), http://dx.doi.org/10.1063/1.3159013. Copyright 2009, AIP Publishing LLC)*

In other reports from literature, the $I - V$ characteristics taken on percolative films of Si NCs dispersed in SiO_2 with different concentration x of Si NCs show different behaviours dependent on the Si NCs density [125−129]. The measurements were performed on samples with planar geometry. In the films with low Si NCs concentration (e.g. $x \approx 20\%$), the NCs are randomly distributed [49], while in the ones with higher concentration between 20% to 75%, the Si NCs are bigger, their diameter increasing from 3.5 to 6.4 nm. They start to form a chain-like percolative network [130] when the concentration exceeds a threshold. The $I - V$ curves taken on films with relatively low Si NCs concentration of 33.7% and 35.7% are linear, and from their analysis the percolation threshold in concentration x_t was found to be 34.7%. By further increasing the Si NCs concentration, the $I - V$ characteristics become superlinear (Fig. 19). The conduction mechanism that explains this behaviour is tunnelling assisted by high electric field, $eV >> k_BT$ [73, 99]. In this case, the charge carriers tunnel the potential barriers produced by the amorphous SiO_2 regions, which separate the Si NCs. The $I - V$ characteristics are described by the formula:

$$I = I_0 \mathrm{sign}(V)\left[\left(1 - |V|/V_0\right) \times \exp\left(-\alpha\sqrt{1 - |V|/V_0}\right) - \exp(-\alpha)\right],$$

where $I_0 = |a|\varphi$, $V_0 = N\varphi/e$, $\alpha = \delta\chi\varphi^{1/2}$, $\chi = (8m_e/\hbar^2)^{1/2}$, the constant a is proportional to the number of equivalent paths of carriers, $\varphi = (2.2 \pm 0.2)$ eV and δ are the height and width of barriers between NCs, N is the number of barriers, e is the elementary charge, m_e is the free electron mass (inside the NC). From the fit of the experimental $I - V$ curves with the above formula (Fig. 19) N and δ were determined for films with different Si NCs concentrations. The authors found a very small number of barriers of tens up to 150 compared with the big number ($\sim 5\times10^3 - 10^4$) of barriers between contacts evaluated from TEM. This is plausible if we consider that carriers choose the path of lowest resistance. On their path the carriers move along the NCs chains and tunnel the potential barriers they found.

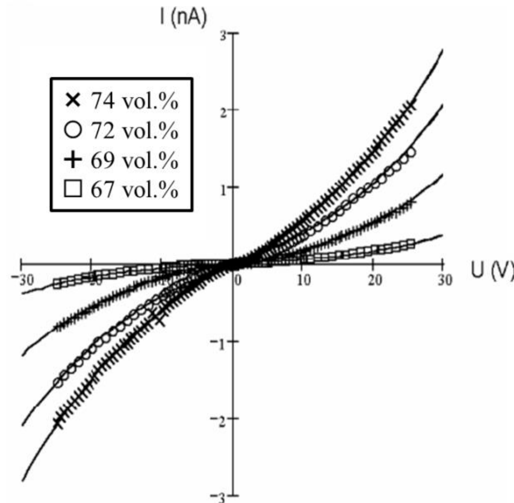

Fig. 19. *Experimental $I - V$ curves (symbols) and fit (model of high electric field- assisted tunnelling) curves (continuous curves) measured on percolative films of Si NCs dispersed in SiO_2 with Si concentrations of 67, 69, 72 and 74 vol. % Si [99]. (Reprinted from Journal of Optoelectronics and Advanced Materials* ***6*** *(1), pages 53-56 (2004), "Conduction mechanisms in silicon-based nanocomposites", V. Iancu, M. Draghici, L. Jdira, M. L. Ciurea, Copyright 2004, with permission from © INOE Publishing House)*

The $I - T$ curves measured on films with middle Si NCs concentration (66%) present Arrhenius dependence with three or two activation energies depending on the bias (4, 5 and 25 V) illustrated in Fig. 20. These activation energies actually represent electric field-assisted transitions between quantum confinement energy levels [36, 73, 131, 132]. At high bias, the smallest activation energy is not observed as at the start temperature of $I - T$ measurement the electrons from the fundamental level are excited to the first excited level by the high electric field.

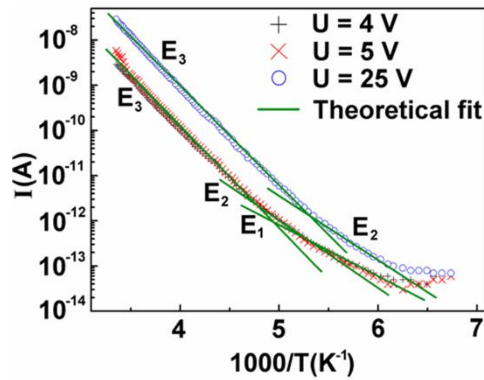

Fig. 20. *I – T curves measured at different biases on films with 66 vol. % Si NCs embedded in SiO_2 [36, 73]. (Reprinted from Chemical Physics Letters, volume **423**, M. L. Ciurea, V. S. Teodorescu, V. Iancu, I. Balberg, Electronic transport in Si–SiO_2 nanocomposite films, pages 225–228, Copyright (2006), with permission from Elsevier)*

In the films with middle Si NCs concentration the voltage percolation thresholds described by a plateau region of current saturation followed by an abrupt current increase were evidenced [126]. In Fig. 21 (left) are presented *I – V* characteristics taken on films with 39.8% and 43.9% Si NCs on which several voltage percolation thresholds are evidenced by arrows. A voltage percolation threshold is related to the opening of a new path with lower resistance, which the carriers choose [133]. At the same time by increasing the voltage, more paths are open including ones with larger barriers (assured by the trapezoidal barrier shape) that are tunnelled by carriers, leading to the abrupt increase of the current.

In contrast, in the *I – V* curves measured in the films with high Si NCs density of 94.89% (Fig. 21 right), the voltage percolation thresholds are no longer observed because all available paths for carrier transport are opened.

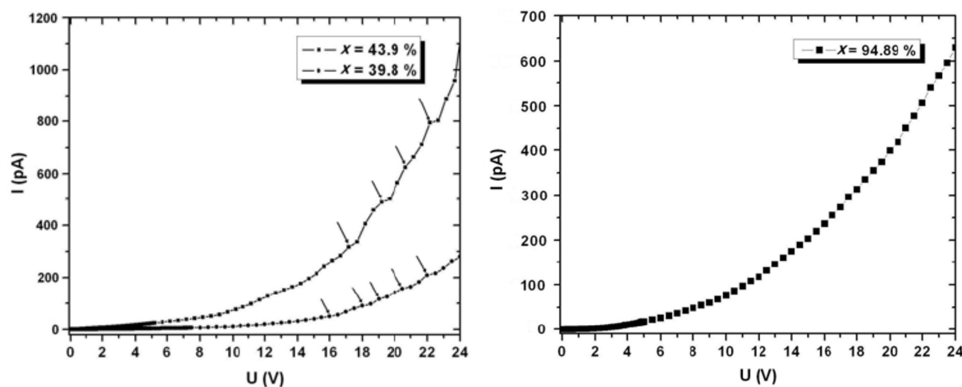

Fig. 21. *I – V curves measured on Si-SiO_2 films with (left) intermediate Si NCs concentrations of 39.8% or 43.9% and (right) high Si NCs concentration of 94.89% [126]. (Reprinted from Journal of Optoelectronics and Advanced Materials **9** (8), pages 2644-2647 (2007), "Percolation phenomena in Si – SiO_2 nanocomposite films", I. Stavarache, M. L. Ciurea, Copyright 2007, with permission from © INOE Publishing House)*

More than that, the initial differential conductance, meaning the derivative of current with respect to voltage calculated at zero voltage, shows a power law dependence according to percolative behaviour, $G_0 \propto (x - x_c)^t$. The exponent t was found to be 0.88 and it was demonstrated to be related to the tunnelling probability P_t according with

$$G_0 \propto P_t \propto P_p \propto (x - x_c)^t ,$$

where P_p is the percolation probability [128].

The transport mechanisms in similar Si-SiO_2 films [70] with Si NCs density very close and above to the percolation threshold were discussed. In the films with high Si NCs concentration the NCs are connected in a network ("touching" NCs), whereas in the films with smaller concentration

than the percolation threshold, most NCs are isolated. The expected percolative behaviour was evidenced by the $\sigma \propto (x - x_c)^t$ power law, x_c being in the range of 30 – 40 vol. % and t between 2 and 4. More, the photoconductivity has a similar dependence on Si NCs concentration [134]. The temperature dependence of conductivity measured in samples with planar geometry of Si-SiO_2 films having Si NCs concentration higher than the percolation threshold and containing Si NCs with size smaller than 10 nm is similar to the one of a disordered semiconductor. The proposed model assumes the presence of band-tail states (due to disorder and doping) with continuous energy distribution. The thermal excitation of carriers takes place from band tail states to the conduction band. This model is sustained by the NCs "touching" characterized by low height and width potential barriers between NCs that act as scattering centers (local potential fluctuations) and not as barriers to be overcome by carriers. On the contrary, in the films with concentration very close to the percolation threshold, the charging effect of NCs was evidenced.

On contrary, Mott variable range-hopping characterized by $\sigma \propto \exp\left(-B/T^{1/4}\right)$ (measured in samples with up-down geometry) taking place through localized states associated with clusters was evidenced in films with different Si vol% concentrations, being formed of ~ 2 nm Si clusters dispersed in SiO_x matrix [116]. The constant B decreases with the increase of Si vol.% concentration explained by the increase of size and/or density of Si clusters with the increase of Si concentration.

Also, from *ab initio* density functional calculations of Si NCs embedded in SiO_2 matrix it is shown that the tunnelling through the potential barriers produced by thin SiO_2 between NCs is dominant [135].

Different tunneling mechanisms were evidenced in multilayers of Si NCs/SiO_2 [72, 81, 136]. So, the direct and phonon assisted tunnelling were evidenced in the structures containing Si NCs that have two diameters of ~3.5 nm and ~5.5 nm. The concentration of smaller NCs is higher than the one of bigger NCs [72]. The $R - T$ characteristics are dependent on the applied gate voltage, so that the curves measured at low voltage have an Arrhenius behaviour with two activation energies, one of few tens of meV at low temperatures and the other one of 100 – 200 meV at high temperatures. The values of the activation energies linearly decrease with the increase of gate voltage. The authors of Ref. [72] describe the electronic structure of NCs by a quantum well with energy levels E_0, E_1 and so on. It is shown that at low temperatures direct tunneling takes place via the first level E_0 (first activation energy), while at high temperatures, phonon-assisted tunneling of carriers occurs via the next level E_1 (second activation energy). More than that, it is demonstrated that only big NCs participate to the charge transport, they being separated by smaller distances. The $I - V$ curves measured at RT at low electric field can be explained only by considering both contributions of direct and phonon-assisted tunneling.

In the multilayers of SiO_2/Si NCs/SiO_2 where Si NCs layers are 2D systems, the transport mechanisms are determined by the thickness of layers [81]. If the SiO_2 layer has 1 nm thickness and Si NCs layer is 3.8 nm thick, the direct and resonant tunnelling are evidenced. Direct tunnelling is evidenced at low voltage and by increasing the voltage resonant tunnelling occurs showing two peaks in the $I - V$ curve (Fig. 22a). The current peaks have small ratios of peak to valley current. For higher voltages, direct tunnelling is enhanced and current peaks are less observable as fewer carriers are available for resonant tunnelling. In multilayers with slightly increased thickness of SiO_2 layer (1.5 nm), the direct tunnelling is restricted, and at higher voltages the trap related tunnelling takes place. In this case, only one current peak is clearly observed, having higher peak to valley current ratio (Fig. 22b). If the SiO_2 and Si NCs layers are much thicker (5.2 nm and 6 nm respectively), then trap related tunnelling is the dominant mechanism because of higher concentration of defects produced during the growth of a thicker SiO_2. More than that, for higher voltages, the Fowler-Nordheim mechanism dominates, and a current peak that appears under resonant tunnelling conditions is evidenced, being much broader. The ratio of peak to valley current is very high because the energy levels in bigger Si NCs are less separated in energy. By analysing all multilayers, the authors observed that the voltages corresponding to the current peaks vary from one structure to another one, and this fact could be due to the wide distribution of Si NCs sizes.

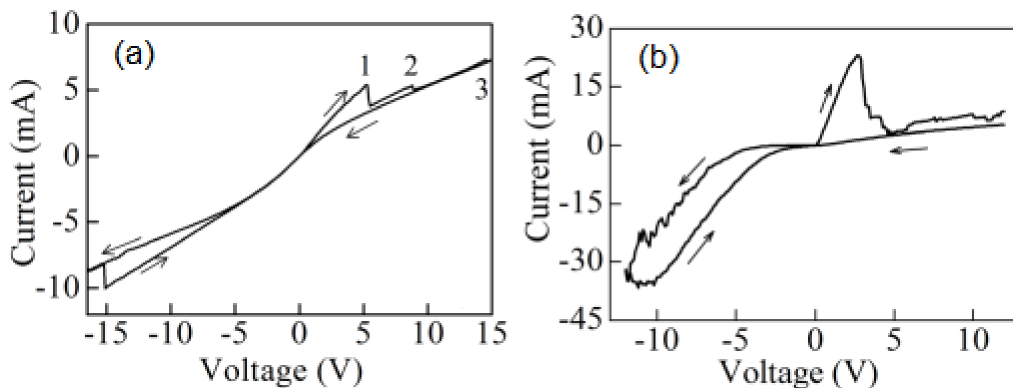

Fig. 22. *I – V curves measured on: (a) multilayers with SiO_2 layers having 1 nm thickness and 3.8 nm thick Si NCs layer; (b) multilayers with slightly increased thickness of SiO_2 (1.5 nm) layer [81]. (Reprinted from D. Y. Chen, Y. Sun, Y. J. He, L. Xu, J. Xu, Journal of Applied Physics **115**, 043703 (2014), http://dx.doi.org/10.1063/1.4861737. Copyright 2014, AIP Publishing LLC)*

The resonant tunnelling mechanism was also found in structures of SiO_2/Si QDs layer/ SiO_2/SiGe QDs layer/SiO_2/Si deposited by low pressure CVD. The Si QDs and SiGe QDs layers as well as the SiO_2 layers are 1D systems [136]. By using an up to down contacts geometry for measurements, it was observed that the tunnelling occurs at the alignment of the second quantum confinement level of Si QD with the first quantum confinement level in SiGe QD.

In multilayered structures formed of 2D array of touching Si NCs separated by SiO_2 layers, the lateral electrical transport and photocurrent mechanisms were studied (Fig. 23) [137]. The structure was grown in five successive steps, in the first one a Si NC layer was deposited by low pressure CVD and subsequently it was thermally oxidized in order to form a dielectric interlayer. This step was five times repeated. The grain boundaries of Si NCs in the Si NCs layers represent scattering centres. The $I – V$ characteristics present at low voltages (~1 V) a linear dependence. For higher voltages a superlinear dependence is observed and the log-log plot gives a slope higher than 2 showing that the space charge limited conduction controlled by traps in Si NCs band gap is dominant.

The $I – T$ curves show at high temperatures a T^{-1} behaviour (thermally excited carriers into the conduction band) and at low temperatures, the current increases more slowly (Fig. 23). At low temperatures the authors of Ref. [137] identified a transport mechanism of hopping assisted by phonons taking place between localized states around Fermi level.

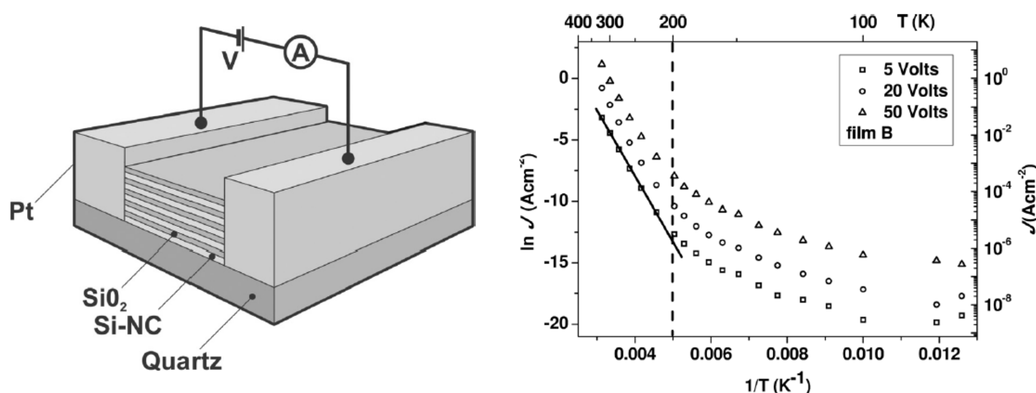

Fig. 23. *(left) Structure for lateral electrical and photocurrent measurements and (right) I – T characteristics on multilayered structures formed of 2D array of touching Si NCs separated by SiO_2 layers [137]. (Reprinted from P. Manousiadis, S. Gardelis, A. G. Nassiopoulou, Journal of Applied Physics **113**, 043703 (2013), http://dx.doi.org/10.1063/1.4789354. Copyright 2013, AIP Publishing LLC)*

The $I_f – V$ measurements performed at 200 K show an ohmic dependence up to 1.5 V and

then a superlinear dependence. In the $I_f - T$ curves, two behaviours were observed, too. At high temperatures, the photocurrent is smaller than the dark current and has a T^{-1} dependence. The $I_f - T$ curve has an activation energy smaller than that in the case of the dark current. At lower temperatures, the photocurrent is higher than the dark current, but is practically constant with temperature, this behaviour being explained by carriers hopping between states with low energy, thus they progressively lose their energy.

A more extended study of photoconductive properties was made in SiO_x (x<2)/SiO_2 multilayers in which different thicknesses of SiO_x layers control the Si NCs sizes [138−141]. The photocurrent spectral distribution curves measured between energies of 1 and 3.75 eV (in lateral geometry) present a broad maximum of which position shifts to higher energies when the NCs size decreases, evidencing the quantum confinement effect in NCs. The curves of I_f dependence on energy E measured at different biases (Fig. 24) show that the photocurrent has two components, one given by carriers tunnelling between Si NCs through the SiO_2 potential barriers and the other one by hopping between defect states present in the SiO_2 matrix. The $I_f - V$ curves measured by illuminating samples with monochromatic light with the wavelength corresponding to the maximum of spectral distribution curve are quasilinear and are explained by carriers transport through Si NCs chains and tunnelling the potential barriers given by thin SiO_2 between NCs. The $I_f - E$ curves show that at high temperatures (100 – 300 K), the maximum shifts to higher energies when the measurement temperature decreases, explained by the NCs gap variation with the temperature, while at low temperatures (13 – 100 K), the maximum position practically does not change. At high temperature, the photocurrent is due to thermionic emission through NCs, while at low temperatures, tunnelling through potential barriers is dominant.

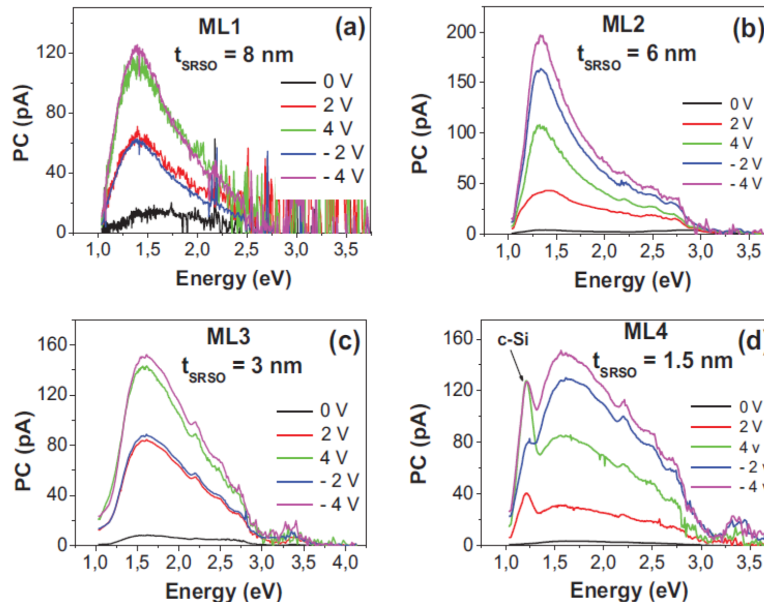

Fig. 24. *The $I_f - E$ curves measured at different biases on SiO_x (x<2)/SiO_2 multilayers with Si-rich silicon oxide (SRSO) layer having different thicknesses of (a) 8 nm, (b) 6 nm, (c) 3 nm, and (d) 1.5 nm [138]. (Reprinted from B. Dridi Rezgui, F. Gourbilleau, D. Maestre, O. Palais, A. Sibai, M. Lemiti, G. Brémond, Journal of Applied Physics **112**, 024324 (2012), http://dx.doi.org/10.1063/1.4737579. Copyright 2012, AIP Publishing LLC)*

4. Conclusions

We have reviewed a number of deposition methods often used for obtaining Ge-SiO_2 and Si-SiO_2 films or multilayers and annealing procedures employed for their nanostructuring. The influence of deposition and annealing conditions on the structure and morphology of resulting films or multilayers formed of Ge or Si NCs/NPs embedded in amorphous SiO_2 matrix was investigated. Special attention has been paid on the changes produced by annealing under

controlled conditions (e.g. temperature and atmosphere) on electrical and photoconductive properties of nanostructures (films and multilayers) related to their morphology and crystalline structure. We have demonstrated the relevance of controlling the deposition and annealing parameters for obtaining films and multilayers with desired structure and targeted electrical and photoconductive properties.

The films with targeted properties can be obtained by tailoring the size of NCs or the thickness of layers which limits the NCs size and by choosing suitable Ge or Si concentration. Magnetron sputtering is succesfully used as deposition method, but other methods such as ion implantation, CVD, sol-gel and MBE are used as well. The annealing under controlled conditions is performed either for nanostructuring of amorphous as-deposited films obtained on substrates maintained at RT or for improving the morphology of films deposited on heated substrates, which usually contain at least clusters or even NCs. The parameters that are efficient in NCs formation are the annealing temperature and atmosphere, but the employed annealing procedure (e.g. in CF or by RTA) is also very important. From this analysis, we can conclude that a special care has to be taken in choosing the proper annealing conditions by considering both processes of diffusion and segregation of Ge or Si that play an esential role in the formation of NCs or NPs.

In the case of Ge, RTA annealing has been proved to be the most efficient in producing Ge NCs at fixed positions in multilayers compared with the annealing in CF at similar temperatures (650 – 700 ^{o}C). In the multilayers annealed in CF, Ge segregates in amorphous NPs located in the middle of SiO_2 layers, while in those annealed by RTA, the amorphous Ge layers are completely transformed in (fixed positioned) NCs. On the contrary in the Ge-SiO_2 films Ge NCs are formed by annealing in CF up to 900 ^{o}C.

In the case of Si-SiO_2 films or Si-rich oxide/SiO_2 multilayers, the annealing in CF or by RTA doesn't influence the formation and size of Si NCs. The optimal temperatures for the formation of Si NCs are between 1000 and 1200 ^{o}C.

Both kinds of films/multilayers containing Ge or Si NCs embedded in SiO_2 matrix present stress field produced by annealing. In SiO_2 films with Ge or Si NCs, the tensile and compressive stress are evidenced together with nanotwins and stacking faults defects and also with dislocations. These defects are produced by the partial relaxation of the stress in the films.

The electrical and photoconductive properties mainly depend on films morphology and structure (NCs size, concentration, separation distance between them and crystallinity) that in turn are produced by the annealing. So, the annealing can tune the electrical and photoconductive properties by changing the transport mechanisms. In contrast, the properties of films or multilayers are weakly dependent on the deposition method, but strongly dependent on the substrate temperature during deposition.

The films based on NCs of Ge or Si embedded in SiO_2 are percolative systems, and therefore, their electrical behaviour is essentially governed by tunnelling or hopping mechanisms in different regimes. The parameters corresponding to the different mechanisms are dependent on the structure characteristics (e.g. NCs diameter, concentration and separation distances). The electrostatic charging and quantum confinement effects play an important role in the nanostructures with Ge or Si NCs.

In the films formed of amorphous Ge NPs, different hopping mechanisms (variable range hopping of Mott and Pollak) govern the electronic charge transport at relatively low temperatures, while at higher temperatures the thermal activation mechanism (Arrhenius dependence) is evidenced. In the films which contain Ge NCs embedded in SiO_2, the charge transport is controlled by tunnelling of carriers, usually between neighbouring Ge NCs, such as thermally activated tunnelling and resonant tunnelling on quantum confinement energy levels of NCs taking into account the single electron charge effect of Ge NCs.

The high photoconductive properties of SiO_2 films with embedded Ge NCs or NPs are mainly produced by quantum confinement effect in NCs and/or by localized states (usually) located at the interface of NC with oxide matrix. The strain can enhance the photoconductive properties. The photosensitivity spectral intervals can be tuned by tailoring NCs size, localized states and strain. The phototransport in the high photoconductive films is due to holes trapping in NCs or on localized states which produces supplementary injection of electrons.

In the films based on amorphous Si NPs embedded in SiO_2, only variable range hopping

(Mott) was observed, whereas in the films with Si NCs, phonon-assisted tunnelling and high electric field-assisted tunnelling, direct and resonant tunnelling between neighbouring NCs are the main transport mechanisms. The carriers tunnel the potential barrier produced by SiO_2 or amorphous grain boundaries between adjacent NCs. These films are also percolative systems, so that the percolative threshold in concentration and percolative voltage thresholds were determined by varying the concentration of NCs. In the films with concentration of NCs higher than the percolation threshold, the electron transitions between quantum confinement energy levels of NCs were evidenced.

The photoconductive properties of Si NCs-based films are also governed by the quantum confinement effect in NCs.

The tunning of the electrical and photoconductive properties by tailoring the morphology and structure (NCs size, concentration, separation distance between them, and crystallinity) offers the possibility to prepare films with desired properties for targeted applications.

Acknowledgements

This work was supported by the Romanian National Authority for Scientific Research through the CNCS–UEFISCDI Contracts No. PN II-PT-PCCA-9/2012 and No. PNII-ID/289-2011.

References

[1] F. Priolo, T. Gregorkiewicz, M. Galli, T. F. Krauss, Nature Nanotech. **9**, 19 (2014).
[2] K. Kim, J. Y. Choi, T. Kim, S. H. Cho, H. J. Chung, Nature **479**, 338 (2011).
[3] R. J. Walters, G. I. Bourianoff, H. A. Atwater, Nature Mater. **4**, 143 (2005).
[4]E. G. Barbagiovanni, D. J. Lockwood, P. J. Simpson, L. V. Goncharova, Appl. Phys. Rev. **1**, 011302 (2014).
[5] S. K. Ray, S. Maikap, W. Banerjee, S. Das, J. Phys. D Appl. Phys. **46**, 153001 (2013).
[6] B. M. Maune, M. G. Borselli, B. Huang, T. D. Ladd, P. W. Deelman, K. S. Holabird, A. A. Kiselev, I. Alvarado-Rodriguez, R. S. Ross, A. E. Schmitz, M. Sokolich, C. A. Watson, M. F. Gyure, A. T. Hunter, Nature **481**, 344 (2012).
[7] W. D. A. M. de Boer, D. Timmerman, K. Dohnalová, I. N. Yassievich, H. Zhang, W. J. Buma, T. Gregorkiewicz, Nature Nanotech. **5**, 878 (2010).
[8] S. Fölsch, J. Martínez-Blanco, J. Yang, K. Kanisawa, S. C. Erwin, Nature Nanotech. **9**, 505 (2014).
[9] L. Pavesi, R. Turan (Eds.), Silicon Nanocrystals: Fundamentals, Synthesis and Applications, Wiley-VCH Verlag GmbH & Co. KGaA, Weinheim (2010).
[10] M. L. Ciurea, V. Iancu, Quantum Confinement in Nanometric Structures, in: D. Baleanu, Z. B. Güvenç and J. A. Tenreiro Machado (Eds.), New trends in nanotechnology and fractional calculus applications, Springer, Dordrecht Heidelberg London New York (2010).
[11] D. Mihalache, J. Optoelectron. Adv. Mater. **13**, 1055 (2011).
[12] L. Sun, J. J. Choi, D. Stachnik, A. C. Bartnik, B. R. Hyun, G. G. Malliaras, T. Hanrath, F. W. Wise, Nature Nanotech. **7**, 369 (2012).
[13] R. Pillarisetty, Nature **479**, 324 (2011).
[14] W. A. Tisdale, K. J. Williams, B. A. Timp, D. J. Norris, E. S. Aydil, X. Y. Zhu, Science **328**, 1543 (2010).
[15] M. Dragoman, G. Konstantinidis, K. Tsagaraki, T. Kostopoulos, D. Dragoman, D Neculoiu, Nanotechnology **23**, 305201 (2012).
[16] M. Dragoman, A. Dinescu, D. Dragoman, Nanotechnology **25**, 415201 (2014).
[17] J. S. Lee, M. V. Kovalenko, J. Huang, D. S. Chung, D. V. Talapin, Nature Nanotech. **6**, 348 (2011).
[18] V. Braic, A. Vladescu, M. Balaceanu, C. R. Luculescu, M. Braic, Surf. Coat. Tech. **211**, 117 (2012).
[19] P. Dimitrakis, P. Normand, V. Ioannou-Sougleridis, C. Bonafos, S. Schamm-Chardon, G. BenAssayag, E. Iliopoulos, Phys. Status Solidi A **210**, 1490 (2013).
[20] L. Khomenkova, B. S. Sahu, A. Slaoui, F. Gourbilleau, Nanoscale Res. Lett. **6**, 172 (2011).
[21] A. Berbezier, J. L. Autran, F. Michelini, Appl. Phys. Lett. **103**, 041113 (2013).

[22] L. Shcherbyna, T. Torchynska, Physica E **51,** 65 (2013).
[23] I. Perez-Wurfl, L. Ma, D. Lin, X. Hao, M. A. Green, G. Conibeer, Sol. Energ. Mat. Sol. Cells **100**, 65 (2012).
[24] M. Brehm, M. Grydlik, Program and book of abstracts of NanoSEA 2014 International Conference, page 83, presented at the 5-th International Conference on Nanostructures Self-Assembly, July 7-11 -th, 2014, Marseille, France.
[25] B. Ghosh, Y. Sakkab, N. Shirahata, J. Mater. Chem. A **1**, 3747 (2013).
[26] C. Y. Chien, W. T. Lai, Y. J. Chang, C. C. Wang, M. H. Kuo, P. W. Li, Nanoscale **6**, 5303 (2014).
[27] S. Cosentino, S. Mirabella, P. Liu, S. T. Le, M. Miritello, S. Lee, I. Crupi, G. Nicotra, C. Spinella, D. Paine, A. Terrasi, A. Zaslavsky, D. Pacifici, Thin Solid Films **548**, 551 (2013).
[28] P. Liu, S. Cosentino, S. T. Le, S. Lee, D. Paine, A. Zaslavsky, D. Pacifici, S. Mirabella, M. Miritello, I. Crupi, A. Terrasi, J. Appl. Phys. **112**, 083103 (2012).
[29] A. M. Lepadatu, I. Stavarache, T. F. Stoica, M. L. Ciurea, Dig. J. Nanomater. Bios. **6**, 67 (2011).
[30] S. Cosentino, E. S. Ozen, R. Raciti, A. M. Mio, G. Nicotra, F. Simone, I. Crupi, R. Turan, A. Terrasi, A. Aydinli, S. Mirabella, J. Appl. Phys. **115**, 043103 (2014).
[31] Ö. Dag, E. J. Henderson, G. A. Ozin, Small **8**, 921 (2012).
[32] S. Parola, E. Quesnel, V. Muffato, J. Bartringer, A. Slaoui, J. Appl. Phys. **113**, 053512 (2013).
[33] L. Khomenkova, Physica B **453**, 19 (2014).
[34] E. Vergara Hernandez, T. V. Torchynska, J. Jedrzejewski, I. Balberg, Physica B **453**, 107 (2014).
[35] M. L. Ciurea, V. Iancu, I. Stavarache, J. Optoelectron. Adv. Mater. **8**, 2156 (2006).
[36] A. M. Lepadatu, I. Stavarache, M. L. Ciurea, V. Iancu, J. Appl. Phys. **107**, 033721 (2010).
[37] M. L. Ciurea, V. Iancu, S. Lazanu, A. M. Lepadatu, E. Rusnac, I. Stavarache, Rom. Rep. Phys. **60**, 735 (2008).
[38] V. Ioannou-Sougleridis, A. G. Nassiopoulou, M. L. Ciurea, F. Bassani, F. Arnaud d' Avitaya, Mater. Sci. Eng. C **15**, 45 (2001).
[39] M. Draghici, M. Miu, V. Iancu, A. Nassiopoulou, I. Kleps, A. Angelescu, M. L. Ciurea, Phys. Status Solidi A **182**, 239 (2000).
[40] M. L. Ciurea, Rom. Rep. Phys. **65**, 841 (2013).
[41] M. L. Ciurea, S. Lazanu, I. Stavarache, A. M. Lepadatu, V. Iancu, M. R. Mitroi, R. R. Nigmatullin, C. M. Baleanu, J. Appl. Phys. **109**, 013717 (2011).
[42] M. Braic, V. Moagar, A. Vladescu, A. Kiss, C. Trisca-Rusu, M. Balaceanu, V. Braic, presented at the International Workshop on Nanostructured Materials, June 21-23 -th, 2006, Antalya, Turkey.
[43] I. Stavarache, A. M. Lepadatu, A. C. Galca, V. S. Teodorescu, M. L. Ciurea, Appl. Surf. Sci. **309**, 168 (2014).
[44] I. Stavarache, A. M. Lepadatu, T. Stoica, M. L. Ciurea, Appl. Surf. Sci. **285**(B), 175 (2013).
[45] I. Stavarache, A. M. Lepadatu, N. G. Gheorghe, R. M. Costescu, G. E. Stan, D. Marcov, A. Slav, G. Iordache, T. F. Stoica, V. Iancu, V. S. Teodorescu, C. M. Teodorescu, M. L. Ciurea, J. Nanopart. Res. **13**, 221 (2011).
[46] B. Zhang, S. Shrestha, M. A. Green, G. Conibeer, Appl. Phys. Lett. **96**, 261901 (2010).
[47] W. K. Choi, H. G. Chew, F. Zheng, W. K. Chim, Y. L. Foo, E. A. Fitzgerald, Appl. Phys. Lett. **89**, 113126 (2006).
[48] F. Gourbilleau, C. Ternon, D. Maestre, O. Palais, C. Dufour, J. Appl. Phys. **106**, 013501 (2009).
[49] V. S. Teodorescu, M. L. Ciurea, V. Iancu, M.-G. Blanchin, J. Mater. Res. **23**, 2990 (2008).
[50] S. Takeoka, M. Fujii, S. Hayashi, Phys. Rev. B **62**, 16820 (2000).
[51] S. Mirabella, S. Cosentino, A. Gentile, G. Nicotra, N. Piluso, L. V. Mercaldo, F. Simone, C. Spinella, A. Terrasi, Appl. Phys. Lett. **101**, 011911 (2012).
[52] S. N. M. Mestanza, E. Rodriguez, N. C. Frateschi, Nanotechnology **17**, 4548 (2006).
[53] M. Yamamoto, T. Koshikawa, T. Yasue, H. Harima, K. Kajiyama, Thin Solid Films **369**, 100 (2000).
[54] T. S. Iwayama, Vacuum **86**, 1634 (2012).
[55] J. I. Wong, T. P. Chen, M. Yang, Y. Liu, C. Y. Ng, L. Ding, J. Appl. Phys. **106**, 013718 (2009).
[56] X. Wang, X. Yu, W.Yu, H. Feng, J. Wang, C. Yin, W. Lu, G. Fu, J. Mater. Sci. **49**, 1353 (2014).

[57] G. Fu, X. Wang, H. Feng, W. Dai, X. Yu, W. Lu, Z. Zhang, W. Yu, Appl. Phys. A **114**, 861 (2014).
[58] T. Dürkop, E. Bugiel, I. Costina, A. Ott, R. Peibst, K. R. Hofmann, Mater. Sci. Eng. B **147**, 213 (2008).
[59] X. X. Wang, J. G. Zhang, L. Ding, B. W. Cheng, W. K. Ge, J. Z. Yu, Q. M. Wang, Phys. Rev. B **72**, 195313 (2005).
[60] S. Cosentino, S. Knebel, S. Mirabella, S. Gibilisco, F. Simone, H. Bracht, G. Wilde, A. Terrasi, Appl. Phys. A. **116**, 233 (2014).
[61] S. Knebel, A. Kyriakidou, H. Bracht, H. Rösner, G. Wilde, Appl. Phys. A **103**, 149 (2011).
[62] G. Das, L. Ferraioli, P. Bettotti, F. De Angelis, G. Mariotto, L. Pavesi, E. Di Fabrizio, G. D. Soraru, Thin Solid Films **516**, 6804 (2008).
[63] R. Aluguri, S. Das, R. K. Singha, S. K. Ray, Curr. Appl. Phys. **13**, 12 (2013).
[64] S. K. Ray, S. Das, R. K. Singha, S. Manna, A. Dhar, Nanoscale Res. Lett. **6**, 224 (2011).
[65] A. Hernández-Hernández, V. T. Rangel-Kuoppa, T. Plach, F. De Moure-Flores, J. G. Quiñones-Galván, J. Santoyo-Salazar, M. Zapata-Torres, L. A. Hernández-Hernández, M. Meléndez-Lira, J. Appl. Phys. **111**, 044327 (2012).
[66] B. Zhang, W. Truong, S. Shrestha, M. A. Green, G. Conibeer, Physica E **45**, 207 (2012).
[67] K. Imakita, M. Ito, M. Fujii, S. Hayashi, J. Appl. Phys. **105**, 093531 (2009).
[68] M. Fujii, O. Mamezaki, S. Hayashi, K. Yamamoto, J. Appl. Phys. **83**, 1507 (1998).
[69] Y. Maeda, Phys. Rev. B **51**, 1658 (1995).
[70] I. Balberg, J. Jedrzejewski, E. Savir, Phys. Rev. B **83**, 035318 (2011).
[71] X. J. Hao, A. P. Podhorodecki, Y. S. Shen, G. Zatryb, J. Misiewicz, M. A. Green, Nanotechnology **20**, 485703 (2009).
[72] V. Osinniy, S. Lysgaard, Vl. Kolkovsky, V. Pankratov, A. Nylandsted Larsen, Nanotechnology **20**, 195201 (2009).
[73] M. L. Ciurea, V. S. Teodorescu, V. Iancu, I. Balberg, Chem. Phys. Lett. **423**, 225 (2006).
[74] M. Dovrat, Y. Oppenheim, J. Jedrzejewski, I. Balberg, A. Sa'ar, Phys. Rev. B **69**, 155311 (2004).
[75] M. Zhang, R. Cai, Y. Zhang, C. Wang, Y. Wang, G. G. Ross, D. Barba, Mater. Charact. **93**, 1 (2014).
[76] L. L. Araujo, R. Giulian, D. J. Sprouster, C. S. Schnohr, D. J. Llewellyn, P. Kluth, D. J. Cookson, G. J. Foran, M. C. Ridgway, Phys. Rev. B **78**, 094112 (2008).
[77] H. Fukuda, T. Kobayashi, T. Endoh, S. Nomura, A. Sakai, Y. Ueda, Appl. Surf. Sci. **130–132**,776 (1998).
[78] Y. Q. Wang, T. Li, W. S. Liang, X. F. Duan, G. G. Ross, Nanotechnology **20**, 315704 (2009).
[79] C. R. Mokry, P. J. Simpson, A. P. Knights, J. Appl. Phys. **105**, 114301 (2009).
[80] L. Ding, T. P. Chen, Y. Liu, M. Yang, J. I. Wong, Y. C. Liu, A. D. Trigg, F. R. Zhu, M. C. Tan, S. Fung, J. Appl. Phys. **101**, 103525 (2007).
[81] D. Y. Chen, Y. Sun, Y. J. He, L. Xu, J. Xu, J. Appl. Phys. **115**, 043703 (2014).
[82] O. Salihoglu, U. Kürüm, H. G. Yaglioglu, A. Elmali, A. Aydinli, J. Vac. Sci. Technol. B **30**, 011807 (2012).
[83] D. Y. Chen, D. Y. Wei, J. Xu, P. G. Han, X. Wang, Z. Y. Ma, K. J. Chen, W. H. Shi, Q. M. Wang, Semicond. Sci. Technol. **23**, 015013 (2008).
[84] N. Daldosso, M. Luppi, S. Ossicini, E. Degoli, R. Magri, G. Dalba, P. Fornasini, R. Grisenti, F. Rocca, L. Pavesi, S. Boninelli, F. Priolo, C. Spinella, F. Iacona, Phys. Rev. B **68**, 085327 (2003).
[85] T. F. Stoica, M. Gartner, V. S. Teodorescu, T. Stoica, J. Optoelectron. Adv. Mater. **9**, 3271 (2007).
[86] N. Chiodini, A. Paleari, M. Catti, S. Brovelli, D. Di Martino, A. Lauria, R. Lorenzi, G. Spinolo, Solid State Commun. **144**, 429 (2007).
[87] H. Yang, X. Yao, S. Xie, X. Wang, S. Liu, Y. Fang, X. Gu, F. Wang, Opt. Mater. **27**, 725 (2005).
[88] H. Yang, X. Yao, X. Wang, S. Xie, Y. Fang, S. Liu, X. Gu, J. Phys. Chem. B **107**, 13319 (2003).
[89] M. Nogami, Y. Abe, Appl. Phys. Lett. **65**, 2545 (1994).
[90] J. A. Rodrıguez, C. Fernández-Sánchez, C. Domınguez, S. Hernández, Y. Berencén, Appl. Phys. Lett. **101**, 171908 (2012).

[91] G. D. Sorarù, S. Modena, P. Bettotti, G. Das, G. Mariotto, L. Pavesi, Appl. Phys. Lett. **83**, 749 (2003).
[92] A. Kanjilal, J. L. Hansen, P. Gaiduk, A. Nylandsted Larsen, P. Normand, P. Dimitrakis, D. Tsoukalas, N. Cherkashin, A. Claverie, Appl. Phys. A **81**, 363 (2005).
[93] L. Feng, J. Zhu, H. Zhu, K. Chen, D. Xu, J. Li, Appl. Phys. A **109**, 547 (2012).
[94] D. Hiller, S. Goetze, M. Zacharias, J. Appl. Phys. **109**, 054308 (2011).
[95] L. V. Titova, T. L. Cocker, D. G. Cooke, X. Wang, Al Meldrum, F. A. Hegmann, Phys. Rev. B **83**, 085403 (2011).
[96] J. Heitmann, F. Muller, L. Yi, M. Zacharias, D. Kovalev, F. Eichholm, Phys. Rev. B **69**, 195309 (2004).
[97] C. L. Yuan, J. G. Chu, W. Lei, Appl. Phys. A **99**, 673 (2010).
[98] A. M. Lepadatu, T. Stoica, I. Stavarache, V. S. Teodorescu, D. Buca, M. L. Ciurea, J. Nanopart. Res. **15**, 1981 (2013).
[99] V. Iancu, M. Draghici, L. Jdira, M. L. Ciurea, J. Optoelectron. Adv. Mater. **6**, 53 (2004).
[100] M. L. Ciurea, E. Pentia, A. Manea, A. Belu-Marian, I. Baltog, Phys. Status Solidi B **195**, 637 (1996).
[101] Y. H. Ye, J. Y. Zhang, X. M. Bao, X. L. Tan, L. F. Chen, Appl. Phys. A **67**, 213 (1998).
[102] S. S. Tzeng, P. W. Li, Nanotechnology **19**, 235203 (2008).
[103] D. Hiller, S. Gutsch, A. M. Hartel, P. Löper, T. Gebel, Margit Zacharias, J. Appl. Phys. **115,** 134311 (2014).
[104] Z. Wan, S. Huang, M. A. Green, G. Conibeer, Nanoscale Res. Lett. **6**, 129 (2011).
[105] V. S. Teodorescu, A. V. Maraloiu, I. Stavarache, A. M. Lepadatu, M. L. Ciurea, Dig. J. Nanomater. Bios. **8**, 1771 (2013).
[106] N. Srinivasa Rao, A. P. Pathak, G. Devaraju, V. Saikiran, Vacuum **85**, 927 (2011).
[107] L. Khriachtchev, T. Nikitin, M. Räsänen, A. Domanskaya, S. Boninelli, F. Iacona, A. Engdahl, J. Juhanoja, S. Novikov, J. Appl. Phys. **108**, 124301 (2010).
[108] I. Bogdanović-Radović, M. Buljan, M. Karlušić, N. Skukan, I. Božičević, M. Jakšić, N. Radić, G. Dražić, S. Bernstorff, Phys. Rev. B **86**, 165316 (2012).
[109] D. Sahin, I. Yildiz, A. I. Gencer, G. Aygun, A. Slaoui, R. Turan, Thin Solid Films **518**, 2365 (2010).
[110] S. R. C. Pinto, A. G. Rolo, M. Buljan, A. Chahboun, S. Bernstorff, N. P. Barradas, E. Alves, R. J. Kashtiban, U. Bangert, M. J. M. Gomes, Nanoscale Res. Lett. **6**, 341 (2011).
[111] I. Stavarache, A. M. Lepadatu, A. V. Maraloiu, V. S. Teodorescu, M. L. Ciurea, J. Nanopart. Res. **14**, 930 (2012).
[112] B. Zhang, Y. Yao, R. Patterson, S. Shrestha, M. A. Green, G. Conibeer, Nanotechnology **22**, 125204 (2011).
[113] M. L. Ciurea, P. Romanian Acad. A **12**, 315 (2011).
[114] M. L. Ciurea, V. Iancu, M. R. Mitroi, Solid State Electron. **51**, 1328 (2007).
[115] G. Zatryb, A. Podhorodecki, J. Misiewicz, J. Cardin, F. Gourbilleau, Nanoscale Res. Lett. **8**, 40 (2013).
[116] M. Fujii, Y. Inoue, H. Shinji, K. Yamamoto, Appl. Phys. Lett. **68**, 3749 (1996).
[117] M. L. Ciurea, I. Stavarache, A. M. Lepadatu, I. Pasuk, V. S. Teodorescu, Phys. Status Solidi B **251**, 1340 (2014).
[118] M. L. Ciurea, V. S. Teodorescu, I. Stavarache, A. M. Lepadatu, GeSiO Based Nanostructures: Electrical Behaviour Related to Morphology and Preparation Method, in: V. Kuncser and L. Miu (Eds.), Size Effects in Nanostructures, Basics and Applications, Springer Ser. Materials, Vol. 205, Springer-Verlag Berlin Heidelberg (2014).
[119] Y. Inoue, M. Fujii, S. Hayashi, K. Yamamoto, Solid State Electron. **42**, 1605 (1998).
[120] S. Cosentino, Pei Liu, S. T. Le, S. Lee, D. Paine, A. Zaslavsky, D. Pacifici, S. Mirabella, M. Miritello, I. Crupi, A. Terrasi, Appl. Phys. Lett. **98**, 221107 (2011).
[121] Z. A. K. Durrani, M. A. Rafiq, Microelectron. Eng. **86**, 456 (2009).
[122] M. A. Rafiq, Y. Tsuchiya, H. Mizuta, S. Oda, Shigeyasu Uno, Z. A. K. Durrani, W. I. Milne, J. Appl. Phys. **100**, 14303 (2006).
[123] M. A. Rafiq, Z. A. K. Durrani, H. Mizuta, A. Colli, P. Servati, A. C. Ferrari, W. I. Milne, S. Oda, J. Appl. Phys. **104**, 123710 (2008).
[124] X. Zhou, K. Usami, M. A. Rafiq, Y. Tsuchiya, H. Mizuta, S. Oda, J. Appl. Phys. **104**, 024518 (2008).
[125] M. L. Ciurea, J. Optoelectron. Adv. Mater. **8**, 13 (2006).

[126] I. Stavarache, M. L. Ciurea, J. Optoelectron. Adv. Mater. **9**, 2644 (2007).
[127] C. Trisca-Rusu, A. C. Nechifor, S. Mihai, C. Parvu, S. I. Voicu, G. Nechifor, 2009 International Semiconductor Conference (CAS), Sinaia, Romania, 2009, Vol. 1 (IEEE, New York, 2009), pp. 285–288.
[128] I. Stavarache, Dig. J. Nanomater. Bios. **6**, 1073 (2011).
[129] L. Baschir, S. Antohe, A. Radu, R. Constantineanu, S. Iftimie, I. D. Simandan, M. Popescu, Dig. J. Nanomater. Bios. **8**, 1645 (2013).
[130] M. L. Ciurea, V. S. Teodorescu, L. C. Nistor, M. G. Blanchin, J. Electrochem. Soc. **146**, 3516 (1999).
[131] V. Iancu, M. R. Mitroi, A. M. Lepadatu I. Stavarache, M. L. Ciurea, J. Nanopart. Res. **13**, 1605 (2011).
[132] M. L. Ciurea, J. Optoelectron. Adv. Mater. **7**, 2341 (2005).
[133] I. Stavarache, A.-M. Lepadatu, V. S. Teodorescu, M. L. Ciurea, V. Iancu, M. Dragoman, G. Konstantinidis, R. Buiculescu, Nanoscale Res. Lett. **6**, 88 (2011).
[134] I. Balberg, E. Savir, J. Jedrzejewski, A. G. Nassiopoulou, S. Gardelis, Phys. Rev. B **75**, 235329 (2007).
[135] K. Seino, F. Bechstedt, P. Kroll, Phys. Rev. B **86**, 075312 (2012)
[136] K. Makihara, M. Ikeda, S. Miyazaki, J. Appl. Phys. **112**, 104301 (2012).
[137] P. Manousiadis, S. Gardelis, A. G. Nassiopoulou, J. Appl. Phys. **113**, 043703 (2013).
[138] B. Dridi Rezgui, F. Gourbilleau, D. Maestre, O. Palais, A. Sibai, M. Lemiti, G. Brémond, J. Appl. Phys. **112**, 024324 (2012).
[139] V. Iancu, M. L. Ciurea, I. Stavarache, V. S. Teodorescu, J. Optoelectron. Adv. Mater. **9**, 2638 (2007).
[140] M. L. Ciurea, M. Draghici, V. Iancu, M. Reshotko, I. Balberg, J. Luminesc. **102-103**, 492 (2003).
[141] V. Iancu, M. L. Ciurea, Solid State Electron. **42**, 1893 (1998).